Adaptive-depth randomized measurement for fermionic observables

Kaiming Bian[1, 2, 3] and Bujiao Wu[1, 2, 3, *]

[1] *Shenzhen Institute for Quantum Science and Engineering, Southern University of Science and Technology, Shenzhen 518055, China*
[2] *International Quantum Academy, Shenzhen 518048, China*
[3] *Guangdong Provincial Key Laboratory of Quantum Science and Engineering, Southern University of Science and Technology, Shenzhen, 518055, China*

Accurately estimating fermionic observables, such as k-RDMs and molecular Hamiltonians, is vital in quantum physics and chemistry. These estimations play a key role in analyzing electronic structures and reaction mechanisms in molecular systems. Fermionic classical shadow (FCS) provides a powerful method to estimate these expectation values without converting them into the Pauli basis. However, implementing FCS requires random matchgate circuits with polynomial depth, which poses a significant challenge for near-term quantum devices due to their limited capabilities. To address this issue, we propose an adaptive-depth fermionic classical shadow (ADFCS) protocol that reduces the depth requirements of FCS while maintaining accuracy. Through theoretical analysis and numerical fitting, we show that the required depth for approximating a Majorana string γ_S—defined as the product of multiple Majorana operators—is proportional to $\max\{\frac{d^2_{\mathrm{int}(S)}}{\log n}, d_{\mathrm{int}}(S)\}$, where $d_{\mathrm{int}}(S)$ represents the minimum distance between indices in set S. Our numerical experiments demonstrate the effectiveness of ADFCS in estimating fermionic observables with varying depths of random matchgate circuits. We further apply the ADFCS protocol to calculate the expectation value of a Kitaev chain Hamiltonian. The results indicate that ADFCS significantly reduces circuit depth requirements while preserving the resource demands on quantum states. Our algorithm may facilitate quantum simulations on near-term devices by reducing circuit depth and addressing gaps between theory and experiment.

I. INTRODUCTION

Simulation of strongly correlated fermionic systems is one of the most important applications of quantum computing [1, 2], highlighting the necessity for advanced measurement techniques in fermionic systems to capture the intricacies of electron correlations and dynamics. An important example of this is the k-reduced density matrix (k-RDM), which efficiently captures the essential features of many-body fermionic systems by focusing on a subset of particles and involves the calculation of various expectation values of fermionic observables. It demonstrates the importance of the efficient calculations of the expectation values in fermionic systems.

The classical shadow (CS) algorithm [3] was introduced to give a classical estimator for a quantum state ρ by employing a random Clifford circuit, measurement in the computational basis, and polynomial classical postprocessing. It is particularly suited for estimating linear properties of ρ, such as the expectation values $\{\mathrm{Tr}(\rho Q_i)\}_{i=1}^m$. The number of measurements required is $\mathcal{O}\left(\max_i \|Q_i\|^2_{\mathrm{shadow}} \log m/\varepsilon^2\right)$, where ε is the desired estimation error and $\|\cdot\|_{\mathrm{shadow}}$ denotes the shadow norm, which depends on the choice of the unitary ensemble. When the unitary ensemble is the global Clifford group, the shadow norm simplifies to $\|Q\|_{\mathrm{shadow}} = \mathrm{Tr}(Q^2)$. Although it is efficient for k-local Pauli observables, it is not efficient for k-local fermionic observables, such as Majorana operators. To address this limitation, fermionic classical shadow (FCS) algorithms [4–6] were developed. These algorithms primarily differ from the CS algorithm by using a Gaussian unitary ensemble rather than the Clifford group for randomness. Both Gaussian unitary and Clifford elements require polynomial-size quantum circuits, which become challenging for near-term quantum devices due to issues like gate noise and limited coherence time [7–12]. In response to this, several approaches have been proposed to design shallow-depth CS protocols [13–15]. However, for FCS side, Zhao et al. [4] have proved that there does not exist subgroup $G \subset \mathrm{Cl}_n \cap \mathbb{M}_n$ which has a better fermionic shadow norm, where Cl_n is the n-qubit Clifford group and $\mathbb{M}_n$ is the matchgate group. An intriguing open question remains:

Is there a shallow-depth FCS algorithm that is efficient for some specific set of fermionic observables and maintains the same sample complexity as the original FCS algorithm?

* wubj@sustech.edu.cn

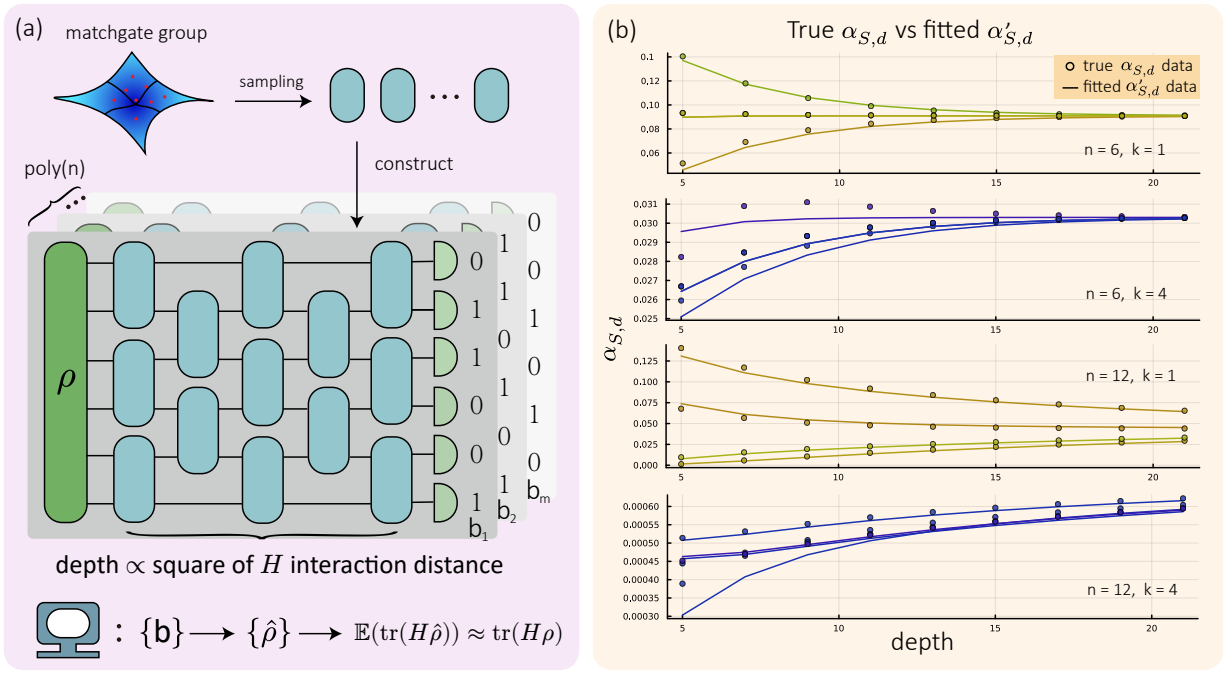

FIG. 1: Illustration of adaptive depth fermionic shallow shadows (ADFCS). (a) The sketch of ADFCS. Unitary gates are independently sampled from the group of two-qubit matchgates and subsequently assigned to each node within the brickwork architecture. Measuring the constructed random circuit multiple times yields a set of bit strings $\{b\}$, which can then be processed on a classical computer. This post-processing step estimates $\mathrm{tr}(H\rho)$ by averaging the expectation values of the classical shadows $\{\hat{\rho}\}$ derived from bit strings $\{b\}$. Depending on the fitting formula of $\alpha_{S,d}$ in Eq. (21), the sampling complexity remains efficient, ensuring the feasibility of the computational process when the depth of random measurement circuit scales proportionally to the square of the interaction distance of the fermionic Hamiltonian $H = \sum c_S \gamma_S$. (b) illustrates the accuracy of the fit $\alpha'_{S,d}$ in comparison to the true value $\alpha_{S,d}$. The results demonstrate that the fitting aligns closely with the true values, particularly when the circuit depth is sufficiently large.

In this study, we delve into the relationship between sample complexity and the depth utilized in constructing the random unitary ensemble. Our analysis focuses on the 1-RDM, leading to an expression that characterizes the connection between sample complexity and the number of layers. Then, we find the relationship for the k-RDM that aligns well with experimental observations. Based on the findings, we investigated the requisite depth of layers necessary to achieve the minimal sample number. Notably, the requisite depth is tight in order [16], indicating that attaining the same lower bound with fewer layers is impossible, thereby providing significant insight into optimizing the depth of random unitary ensembles for practical quantum computing applications.

We propose adaptive-depth fermionic classical shadow (ADFCS) alogrithm for optimizing the depth of the brickwork random matchgate circuit, as shown in Fig. 1(a). Given a observable H, the circuit depth d^* is adaptive selected by interaction distance of the observable. The interest state ρ is measured on computational basis after d^*-depth random matchgate circuit $U_{Q_{d^*}}$. Then the expectation value $\mathrm{Tr}(\rho H)$ is estimated by the measurement outcomes. We compare the ADFCS and FCS with typical observable γ_S and the Kiteav chain Hamiltonian H_K. For both cases, the ADFCS achieve similar precise with d^* depth. Since every matchgate circuit could be achieve by n^2 size remote connection circuit, which indicates that every matchgate circuit could be achieve by n^2 depth brickwork circuit. It suggets that the Haar random matchgate circuit requires $\Omega(n^2)$ depth, while $d^* = \mathcal{O}(n^2)$. We conclude that the ADFCS achieve similar results with relative shallow depth with brickwork architecture.

II. PRELIMINARY

Notations. We utilize $\mathcal{H}$ to denote the quantum state Hilbert space, and $\mathcal{L}(\mathcal{H})$ to denote the linear operator space which operates on Hilbert space $\mathcal{H}$. Quantum channel $\Lambda \in \mathcal{L}(\mathcal{L}(\mathcal{H}))$ is a superoperator that maps a linear operator into another. For convenience, we introduce the Pauli-transfer matrix (PTM) representation, which expresses both

superoperators and operators in terms of their action on the Pauli basis. A non-zero linear operator $|A\rangle\rangle$ can be vectorized as $|A\rangle\rangle := \frac{A}{\sqrt{\mathrm{Tr}(A^\dagger A)}}$ where the normalization ensures that it is properly scaled. The inner product between the vectorized formation of two operators $A, B \in \mathcal{L}(\mathcal{H})$ is defined as $\langle\langle A|B\rangle\rangle := \frac{\mathrm{Tr}\left(A^\dagger B\right)}{\sqrt{\mathrm{Tr}(A^\dagger A)\mathrm{Tr}(B^\dagger B)}}$. Specifically, for the Majorana observable γ_S, the vectorized form is $|\gamma_S\rangle\rangle = \frac{\gamma_S}{\sqrt{2^n}}$, where n is the number of qubits. The superoperator Λ can be represented as a matrix in Pauli basis. Its operating on a linear operator $A \in \mathcal{L}(\mathcal{H})$ can be denoted as $\Lambda|A\rangle\rangle := \frac{\Lambda(A)}{\sqrt{\mathrm{Tr}(A^\dagger A)}}$. Further details on the Pauli-transfer matrix representation can be found in Appendix A.

Majorana operators and matchgate circuits. Studying Majorana operators in fermionic systems is crucial as they underpin the behavior of these systems and have numerous applications, including calculating the expectation values of Majorana operators, such as the energy related to the fermionic Hamiltonian and all elements of k-RDM. The Majorana operators can be defined as

$$\gamma_{2j-1} := a_j + a_j^\dagger, \quad \gamma_{2j} := -\mathsf{i}\left(a_j - a_j^\dagger\right), \tag{1}$$

where $a_j, a_j^\dagger$ are the annihilation and creation operators for the j-th site respectively. Observables in fermionic systems can be expressed as the linear combination of the products of Majorana operators [17]

$$\gamma_S := \gamma_{i_1}\gamma_{i_2}\cdots\gamma_{i_{|S|}}, \tag{2}$$

where $i_1 < i_2 < \cdots < i_{|S|}$, and $S = \{i_1, i_2, \cdots, i_{|S|}\}$. Especially, we set $\gamma_\emptyset$ be the identity operator $\mathbb{1}$ when S is the empty set $\emptyset$. A Majorana operator can be represented in Pauli formation as $\gamma_{2j-1} = \left(\prod_{i=1}^{j-1} Z_i\right) X_j$, $\gamma_{2j} = \left(\prod_{i=1}^{j-1} Z_i\right) Y_j$, for any $j \in [2n]$.

Except for the standard Majorana operators in Eq. (1), there are different bases to express the fermionic Hamiltonian. Different bases could be obtained by the orthogonal transformation of the standard Majorana operators $\tilde{\gamma}_\mu = \sum_{\nu=1}^{2n} Q_{\mu\nu}\gamma_\nu$, where Q is a real orthogonal matrix, $Q \in O(2n)$. The different sets of bases $\{\tilde{\gamma}_\mu\}$ are also called the Majorana operators because they satisfy the same anti-commutation relation $\{\gamma_\nu, \gamma_\mu\} = 2\delta_{\mu\nu}$. The orthogonal linear combinations of Majorana operators can be represented as unitary

$$U_Q^\dagger \gamma_\mu U_Q = \sum_{\nu=1}^{2n} Q_{\mu\nu}\gamma_\nu = \tilde{\gamma}_\mu, \tag{3}$$

where the unitaries U_Q are called fermionic Gaussian unitaries. Followed by Eq. (3), the fermionic Gaussian unitary preserves the cardinality $|S| = \#\{i \mid i \in S\}$ of γ_S, which can be expressed as $U_Q^\dagger \gamma_S U_Q = \sum_{|S'|\in\binom{[2n]}{|S|}} \det\left(Q|_{S,S'}\right)\gamma_{S'}$. The set $\binom{[2n]}{|S|}$ represents the collection of all subsets of $\{1, 2, \ldots, 2n\}$ that contain exactly $|S|$ elements, and the matrix $A|_{S,S'}$ is obtained from the matrix A by selecting the rows indexed by the set S and the columns indexed by the set S'. For simplicity, we refer to a Majorana string γ_S with $|S| = k$ as a *k-local Majorana string* throughout this manuscript.

Matchgate circuits are the quantum circuit representation of fermionic Gaussian unitaries [6]. The collection of all n-qubit matchgate circuits constitutes the matchgate group $\mathbb{M}_n$. This group is generated by rotations of the form $\exp\left(\mathsf{i}\theta X_\mu X_\nu\right), \exp\left(\mathsf{i}\theta Z_\mu\right)$ and X_n, where θ is a real parameter, and μ, ν are indices corresponding to nearest-neighbor qubits in a linear arrangement. Notably, operations within the matchgate group can be efficiently simulated on a classical computer. This efficiency arises because the action of a matchgate circuit U_Q corresponds to Givens rotations associated with an orthogonal matrix Q, facilitating polynomial-time classical simulation [9, 18].

We present the twirling of the matchgate group in the following lemma, as it is utilized in the proof of our main results.

Lemma 1 (The three moments of uniform distribution in $\mathbb{M}_n$, Ref. [6])**.** *The k-moment twirling $\mathcal{E}^{(j)}$ is defined by*

$$\mathcal{E}^{(j)}(\cdot) := \int_{U_Q\in\mathbb{M}_n} \mathrm{d}U_Q \; U_Q^{\otimes j}(\cdot)U_Q^{\dagger\otimes j}. \tag{4}$$

The first three moments are

$$\begin{aligned}\mathcal{E}^{(1)} &= |\mathbb{1}\rangle\rangle\langle\langle\mathbb{1}| \\ \mathcal{E}^{(2)} &= \sum_{k=0}^{2n}\binom{2n}{k}^{-1}\sum_{S,S'\subseteq[2n]}|\gamma_S\rangle\rangle|\gamma_S\rangle\rangle\langle\langle\gamma_{S'}|\langle\langle\gamma_{S'}| \\ \mathcal{E}^{(3)} &= \sum_{\substack{k_1,k_2,k_3\in[2n]\\ k_1+k_2+k_3\leq 2n}}|\mathcal{R}\rangle\rangle\langle\langle\mathcal{R}|,\end{aligned} \tag{5}$$

where

$$|\mathcal{R}\rangle\rangle = \binom{2n}{k_1,k_2,k_3,2n-k_1-k_2-k_3}^{-1/2}\sum_{\substack{A,B,C\,disjoint\\ |A|=k_1,|B|=k_2,|C|=k_3}}|\gamma_A\gamma_B\rangle\rangle|\gamma_B\gamma_C\rangle\rangle|\gamma_C\gamma_A\rangle\rangle. \tag{6}$$

(Fermionic) classical shadow protocol. The classical shadow (CS) process involves randomly applying a unitary $\mathcal{U}$ from some unitary ensemble $\mathbb{U}$ (such as the Clifford group) on a quantum state ρ, followed by measurement in computational bases, yielding outcomes $|b\rangle\rangle$ that form a classical description of ρ, known as "*classical shadow*", denoted as $|\hat{\rho}\rangle\rangle = \mathcal{M}_{\rm CS}^{-1}\mathcal{U}^{-1}|b\rangle\rangle$, where $\mathcal{M}_{\rm CS} := \mathbb{E}_{\mathcal{U}\in\mathbb{U}}\left[\mathcal{U}^\dagger\sum_b|b\rangle\rangle\langle\langle b|\mathcal{U}\right]$. By choosing $\mathbb{U}$ as Clifford group Cl_n, the classical shadow channel can be simplified to $\mathcal{M}_{\rm CS} = \Pi_0 + \frac{1}{2^n+1}\Pi_1$, where Π_0 is the projector onto the identity subspace and Π_1 is the projector onto the subspace spanned by all Pauli bases except identity [3, 19]. This simple representation allows efficient construction of the classical shadow $\hat{\rho}$.

In the framework of FCS, the shadow channel $\mathcal{M}_{\rm FCS} := \mathbb{E}_{Q\in O(2n)}\left[\mathcal{U}_Q^\dagger\sum_b|b\rangle\rangle\langle\langle b|\mathcal{U}_Q\right]$ is not invertible across the entire Hilbert space. Its invertibility is constrained to a subspace spanned by even operators, denoted as $\Gamma_{\rm even} := \mathrm{span}\{\gamma_S \mid |S| = 2j, j = 0,1,2,\cdots,n\}$. For set S with odd cardinality, the channel $\mathcal{M}_{\rm FCS}(\gamma_S) = 0$, rendering these components inaccessible.

As a result, FCS is limited to recovering expectation values of observables that reside within the $\Gamma_{\rm even}$ subspace. However, this restriction is sufficient for capturing physical observables, as they are typically even operators due to the conservation of fermionic parity [20]. Unless otherwise specified, all discussions and calculations are assumed to take place within the $\Gamma_{\rm even}$.

III. ADAPTIVE-DEPTH FERMIONIC CLASSICAL SHADOWS

Here we consider the adaptive-depth fermionic classical shadow (ADFCS) by selecting the unitary ensemble as d-depth local matchgates with brickwork architecture, as shown in Fig. 1(a), which is widely applied in superconducting quantum devices [10]. It has been shown that certain observables cannot be addressed by replacing the global $\mathrm{Cl}_n\cap\mathbb{M}_n$ group with shallow-depth local matchgate circuits [4]. However, it remains open when global elements are necessary and how to efficiently generate the expectation values of a given set of fermionic observables using the shallowest depth matchgate circuits while minimizing the number of samplings. Here, we address this question by exploring the relationship between the number of required measurements and the depth of the matchgate circuit for some specific set of fermionic observables using the brickwork architecture. Our approach introduces a d-depth ADFCS channel to estimate $\mathrm{Tr}\left(\rho\gamma_S\right)$ for any quantum state ρ. We then determine the optimized depth order for the expectation values of the specific fermionic observables $\mathrm{Tr}\left(\rho\gamma_S\right)$ with respect to an unknown quantum state ρ prepared by a quantum device.

A. Shadow channel analysis in ADFCS

For simplicity, we utilize U_{Q_d} to denote a d-depth matchgate circuit with brickwork structure, and $\mathbb{U}_{Q_d}$ to denote the set of all d-depth matchgate circuit throughout this manuscript. We denote $\mathcal{M}_d$ as the d-depth ADFCS shadow channel, which maps a quantum state ρ to

$$\mathcal{M}_d(\rho) := \mathop{\mathbb{E}}_{U\in\mathbb{U}_{Q_d},b\in\{0,1\}^n}\left[\langle b|U_{Q_d}\rho U_{Q_d}^\dagger|b\rangle U_{Q_d}^\dagger|b\rangle\langle b|U_{Q_d}\right]. \tag{7}$$

Due to the expectation property of the subset $\mathbb{U}_{Q_d}$, the Majorana operator remains invariant under the action of $\mathcal{M}_d$, apart from a scaling factor $\alpha_{S,d}$, i.e.,

$$\mathcal{M}_d(\gamma_S) = \alpha_{S,d}\gamma_S, \tag{8}$$

where $\alpha_{S,d} := \int \mathrm{d}U_{Q_d} \left| \langle \mathbf{0}| U_{Q_d}\gamma_S U_{Q_d}^\dagger |\mathbf{0}\rangle \right|^2$. The proof is shown in Appendix B.

Eq. (8) provides an explicit expression for the shadow channel, enabling a detailed analysis of the statistical properties of ADFCS. The ADFCS estimator is an unbiased estimator, analogous to the FCS estimator, which follows directly from the linearity of the shadow channel $\mathcal{M}_d$

$$\mathop{\mathbb{E}}_{U_{Q_d},b}(\mathcal{M}_d^{-1}(U_{Q_d}^\dagger |b\rangle \langle b| U_{Q_d})) = \mathcal{M}_d^{-1}(\mathbb{E}(U_{Q_d}^\dagger |b\rangle \langle b| U_{Q_d})) = \rho \tag{9}$$

when $\alpha_{S,d}$ is non-zero.

For any observable γ_S and an unknown quantum state ρ, the variance of the ADFCS estimator $v = \mathrm{Tr}(\hat{\rho}\gamma_S)$ is bounded as follows:

$$\mathrm{Var}[v] \leq \frac{1}{\alpha_{S,d}}. \tag{10}$$

The detailed derivation of Eq. (10) is provided in Appendix C. Using this result and applying Chebyshev's inequality, the estimation error $|v - \mathrm{Tr}(\rho\gamma_S)|$ can be bouned to ϵ using $\frac{1}{\alpha_{S,d}\epsilon^2}$ copies of the quantum states with high success probability. In the following sections, we will present the calculation for $\alpha_{S,d}$, along with its upper bound.

B. Tensor Network Approach to Variance Bound

By Equation (10), bounding the variance requires calculating $\alpha_{S,d}$. Here we demonstrate that $\alpha_{S,d}$ can be represented as a tensor network and computed through contraction. Using the Pauli-transfer matrix representation, $\alpha_{S,d}$ can be expressed as

$$\alpha_{S,d} = \langle\langle \mathbf{0}, \mathbf{0}| \int \mathrm{d}\mathcal{U}_{Q_d}\mathcal{U}_{Q_d}^{\otimes 2}|\gamma_S, \gamma_S\rangle\rangle, \tag{11}$$

where $\mathcal{U}_{Q_d}$ is the super operator of U_{Q_d}, $\mathcal{U}_{Q_d}|\gamma_S\rangle\rangle = U_{Q_d}\gamma_S U_{Q_d}^\dagger$. Consequently, the integration over $\mathcal{U}_{Q_d}$ can be broken down into a product of a series of integrations over these independent 2-qubit matchgates. By Lemma 1, we can represent the integration over each 2-qubit matchgate as a fourth-order tensor $\mathcal{T}$ with indices $\sigma_1, \sigma_2, \sigma_3, \sigma_4$. The explicit form of this tensor is given by

$$\mathcal{T}^{\sigma_1\sigma_2}_{\sigma_3\sigma_4} := \langle\langle \sigma_1, \sigma_2|\langle\langle \sigma_1, \sigma_2| \int_{Q\sim O(4)} \mathrm{d}\mathcal{U}_Q\mathcal{U}_Q^{\otimes 2}|\sigma_3, \sigma_4\rangle\rangle|\sigma_3, \sigma_4\rangle\rangle, \tag{12}$$

where the index $\sigma_1, \sigma_2, \sigma_3, \sigma_4$ of tensor $\mathcal{T}$ represent the Pauli operators. The tensor $\mathcal{T}$ is the integration of one blue random gate in Fig. 1. By connecting these tensors $\mathcal{T}$ in the same brickwork architecture as U_{Q_d}, the integration over the superoperator can be transformed into a tensor network. The transformation details are shown in Appendix D.

The value of $\alpha_{S,d}$ can be calculated by contracting the corresponding brickwork tensor network, which is shown in Fig. 2(a). Specifically, the brickwork tensor network, denoted as $\mathcal{C}$, is contracted with $\langle\langle \mathbf{0}, \mathbf{0}|$ and $|\gamma_S, \gamma_S\rangle\rangle$ in the Pauli-transfer matrix (PTM) representation to compute $\alpha_{S,d}$

$$\alpha_{S,d} = \langle\langle \mathbf{0}, \mathbf{0}|\mathcal{C}|\gamma_S, \gamma_S\rangle\rangle. \tag{13}$$

Following the proof of Lemma 5 in Ref. [13], the tensor network $\mathcal{C}$ could be represented by a matrix product operator with bond dimension $2^{\mathcal{O}(d)}$. It suggests that calculating $\alpha_{S,d}$ by tensor network contraction is efficient only when the depth d is shallow.

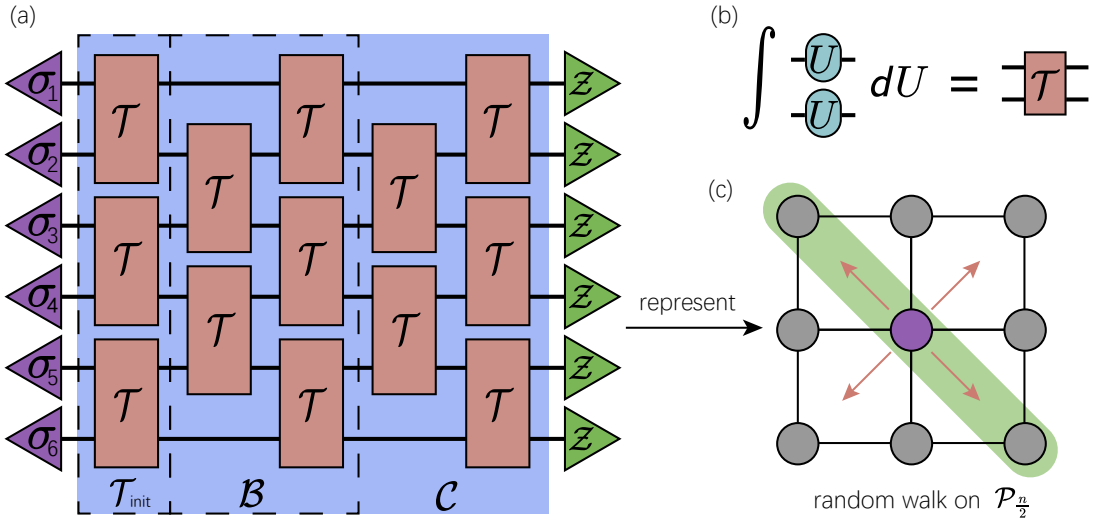

FIG. 2: Representing the tensor contraction of $\mathcal{C}$ to the random walk on the polynomial space $\mathcal{P}_{\frac{n}{2}}$. (a) shows the tensor network for computing $\alpha_{S,d}$. The purple triangles are Pauli operators corresponding to γ_S via Jordan-Wigner transformation. The green triangles $\mathcal{Z}$ represent the supervector $\frac{1}{2}(|\mathbb{1},\mathbb{1}\rangle\rangle + |Z,Z\rangle\rangle)$. (b) draws the definition of $\mathcal{T}$ in Eq. (12). We represent the contraction of $\mathcal{C}$ to the polynomial space $\mathcal{P}_{\frac{n}{2}}$ in (c). Transitioning the state $|\gamma_S,\gamma_S\rangle\rangle$ and contracting it by $\mathcal{Z}$ is equivalent to summing the probability over the diagonal sites in a 2D random walk. The sites (i,j) in $\mathcal{P}_{\frac{n}{2}}$ are the term y_iy_j.

C. Adaptive depth for two-local Majorana strings

Here we start by determining the minimum depth d for the matchgate subset $\mathbb{U}_{Q_d}$, such that the variance of the 2-local Majorana string γ_S requires the same or fewer measurements compared to the full matchgate group $\mathbb{M}_n$. Notably, for certain γ_S, the optimized number of measurements can be significantly improved compared to FCS when using a smaller d. As an instance, suppose we need to estimate the expectation of $\gamma_i\gamma_{i+1}$. The random measurement in FCS actually shuffles the $\gamma_i\gamma_{i+1}$ to any $\gamma_j\gamma_k$ uniformly. However, a matchgate circuit with $d=2$ will only slightly perturb the $\gamma_i\gamma_{i+1}$ to the nearby operators $\{\gamma_j\gamma_k \mid i-2\le j\le i+2, i-1\le k\le i+3\}$. A smaller sample space allows it to approach its theoretical mean with fewer samples compared to the FCS method.

We will investigate how the sample complexity of the quantum state changes with increasing depth of the matchgate layers. To determine the circuit layer requirements for efficient measurement of a fixed 2 local Majorana string γ_S, we derive an expression for $\alpha_{S,d}$ and identify the optimal depth d^* such that $\alpha_{S,d^*}=\frac{1}{\text{poly}(n)}$. It is challenging to give the explicit formulation of the $\alpha_{S,d}$ using the tensor network contraction. However, we could simplify the calculation by restricting the action of the tensor within the subspace spanned by $\Gamma_2 := \text{span}\{\gamma_S \mid |S|=2\}$. By restricting the input state of the whole tensor network $\mathcal{C}$ to the subspace Γ_2, we can introduce more refined structures by mapping this subspace to a polynomial space. This isomorphism allows us to analyze the system more effectively. We observed that the tensor network contraction of $\mathcal{C}$ in Γ_2 is analogous to a random walk in polynomial space.

We will focus on random matchgate circuits characterized by an even number of qubits and an odd circuit depth. For the random matchgate circuits with this structure, the contraction of $\mathcal{C}$ can be represented within the space of quadratic polynomials with $\frac{n}{2}$ variables. For the circuits with even circuit depth, the contraction can be analyzed using a similar method. Denote the quadratic polynomial representation space as $\mathcal{P}_{\frac{n}{2}}$, the contraction of $\mathcal{C}$ could be described by the random walk with a simple pattern in space $\mathcal{P}_{\frac{n}{2}}$.

To represent this random walk, we use the transition process $\mathcal{B}$ to denote a pair of successive gate layers starting from an odd layer,

$$\mathcal{B}|\gamma_S,\gamma_S\rangle\rangle = \sum_{S':|S'|=|S|} \text{Prob}(\gamma_{S'}|\gamma_S)|\gamma'_S,\gamma'_S\rangle\rangle, \tag{14}$$

which is shown in Fig. 2(a). The contraction of $\mathcal{C}$ can be understood as the repeated application of $\mathcal{B}$ to the state $|\gamma_S\rangle\rangle$. As previously mentioned, we focus on the circuit with odd depth. Therefore, the entire tensor network can be expressed as

$$\mathcal{C} = \mathcal{B}^{\lfloor d/2\rfloor}\,\mathcal{T}_{\text{init}}, \tag{15}$$

where $\mathcal{T}_{\text{init}} = \mathcal{T}^{\otimes \frac{n}{2}}$ (and the circuit can be expressed as $\mathcal{C} = \mathcal{B}^{d/2}$ if the depth is an even number). Each $\mathcal{B}$ corresponds to a single transition step in a random walk. Therefore, the entire tensor network $\mathcal{C}$ represents a random walk starting from γ_S and taking $\lfloor \frac{d}{2} \rfloor$ steps, which is shown in Fig. 2(c). The details of mapping the tensor contraction of $\alpha_{S,d}$ to the random walk in $\mathcal{P}_{\frac{n}{2}}$ is shown in Appendix E.

We observe that the random walk follows the pattern of a symmetry lazy random walk (SLRW) [21, 22] almost everywhere within the Γ_2 space. SLRW is a stochastic process in which the walker has a probability of staying in the same position at each step and equal probabilities of moving to neighboring positions. Firstly, we consider the SLRW across the subspace Γ_2 adheres to the SLRW

$$\mathcal{L}_{\Gamma_2}|\gamma_S, \gamma_S\rangle\rangle = \sum_{S':|S'|=|S|} \text{Prob}_L(\gamma_{S'}|\gamma_S)|\gamma'_S, \gamma'_S\rangle\rangle, \tag{16}$$

where $\mathcal{L}_{\Gamma_2}$ is the transition operator in SLRW, and the concrete form of $\mathcal{L}_{\Gamma_2}$ is shown in Appendix E 2, Eq. (E20). We replace the transition operator $\mathcal{B}$ with the SLRW transition operator $\mathcal{L}_{\Gamma_2}$ in $\mathcal{C}$ and use the transition $\mathcal{L}_{\Gamma_2}$ to calculate the tensor network contraction

$$\alpha^L_{S,d} = \langle\langle \mathbf{0}, \mathbf{0}|\mathcal{L}^{\lfloor \frac{d}{2} \rfloor}_{\Gamma_2}\mathcal{T}_{\text{init}}|\gamma_S, \gamma_S\rangle\rangle. \tag{17}$$

As we have shown in Table II of Appendix E, the transition result of $\mathcal{L}_{\Gamma_2}$ equals $\mathcal{B}$ for most states in Γ_2, this indicates that the variable $\alpha^L_{S,d}$ likely constitutes the dominant contribution to $\alpha_{S,d}$. Additionally, numerical fitting further confirms that $\alpha_{S,d}$ is primarily governed by $\alpha^L_{S,d}$, as shown in Fig. 1 (b).

There is a known analytical propagation equation for the SLRW [21]. By applying this propagation equation and making certain approximations, the α-value can ultimately be expressed as a Poisson summation

$$\alpha^L_{S,d} = \frac{1}{3\sqrt{\pi(d-1)}} \sum_{k=-\infty}^{\infty} \left(e^{-\frac{(kn+a)^2}{d-1}} + e^{-\frac{(kn+b)^2}{d-1}} \right) + \mathcal{O}(e^{-\frac{\pi^2 d}{2}}). \tag{18}$$

In Eq. (18), we denote the Majorana observable γ_S with $|S| = 2$ as $\gamma_i\gamma_j$, the variable a, b are defined by $a := ||\lfloor \frac{i-1}{4} \rfloor - \lfloor \frac{j-1}{4} \rfloor|$, and $b := \lfloor \frac{i-1}{4} \rfloor + \lfloor \frac{j-1}{4} \rfloor + 1$. We leave the detailed proof of Eq. (18) to Appendix F.

We aim to estimate the order of $\alpha_{S,d}$ by $\alpha^L_{S,d}$, which could be achieved by bounding the ratio $\alpha_{S,d}/\alpha^L_{S,d}$ to a constant value. To bound the ratio, we introduce an auxiliary function

$$\Delta(S, S', d) = \langle\langle \gamma_{S'}, \gamma_{S'}|\mathcal{B}^{\lfloor \frac{d}{2} \rfloor}\mathcal{T}_{\text{init}} - \mathcal{L}^{\lfloor \frac{d}{2} \rfloor}_{\Gamma_2}\mathcal{T}_{\text{init}}|\gamma_S, \gamma_S\rangle\rangle, \tag{19}$$

where $S' \in \Gamma_2$. Recall that the operator $\gamma_{S'}$ is defined as $\gamma_{S'} = \gamma_u\gamma_v$ where $S' = \{u, v\}$. In numerical experiments, we observe that the term $\Delta(S, S', d)$ is non-negative if and only if the element u is close to v for $S' = \{u, v\}$ and any S, d, as shown in Fig. 7 of Appendix G. Based on this finding, we show that the ratio $\alpha_{S,d}/\alpha^L_{S,d}$ can be bounded by a constant value. The concrete description for bounding the ratio $\alpha_{S,d}/\alpha^L_{S,d}$ is provided in Appendix G.

The relation between $\alpha^L_{S,d}$ and $\alpha_{S,d}$, named $\alpha^L_{S,d} \geq c\alpha^L_{S,d}$ for constant c, indicated that the order of $\alpha^L_{S,d}$ consistent with the order of $\alpha_{S,d}$. Here, we propose the adaptive depth d^* of a random matchgate circuit by analyzing the order of $\alpha^L_{S,d}$. By Eq. (18), for $a = \mathcal{O}(\text{polylog}(n))$ and the measurement depth $d = \text{polylog}(n)$ can yield a polynomially small $\alpha_{S,d} = \Omega(1/\text{poly}(n))$, we postpone the proof in Appendix H. Otherwise, if $a = \Omega(\text{polylog}(n))$, achieving a polynomially small $\alpha_{S,d}$ (rather than an exponentially small one) requires a measurement circuit with depth of $d = \Omega\left(\frac{(i-j)^2}{\log(n)}\right)$. Thus, we could adaptively select the depth d based on the distance $|i-j|$,

$$d^* = \Theta\left(\max\left\{\frac{(i-j)^2}{\log(n)},\ |i-j|\right\}\right). \tag{20}$$

By Eq. (18), if the depth of the matchgate circuit $d = o(d^*)$, the value of $\alpha^L_{S,d}$ will be exponentially small, indicating that exponential samples are required to obtain a good estimation of the expectation value.

D. Adaptive depth for general k local Majorana strings

Here we focus on the extension of adaptive depth to general k-local Majorana strings for constant k. Fermionic observables generated by k-local Majorana strings for constant k play a critical role in various quantum models across physics and chemistry. These operators are essential in describing physical observables such as interaction

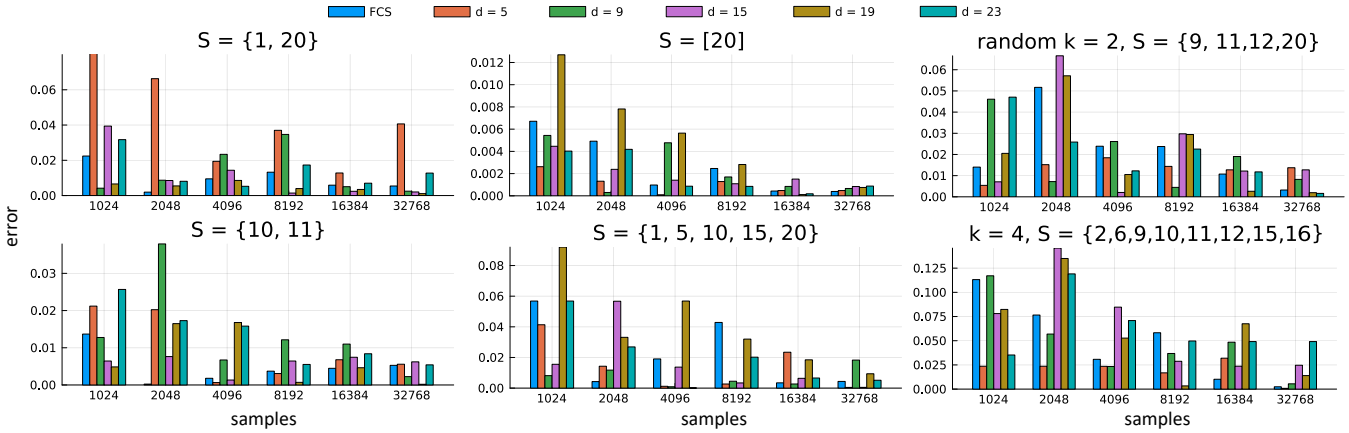

FIG. 3: Numerical simulation comparing FCS and ADFCS performance. A quantum state ρ of 10 qubits is randomly initialized, and both FCS and ADFCS methods are used to estimate the expectation values of γ_S for different S. The x-axis represents the number of samples R, while the y-axis shows the absolute error between the estimated expectation $\frac{1}{R}\sum_i \mathrm{Tr}(\hat{\rho}_i\gamma_S)$ and the true expectation $\mathrm{Tr}(\rho\gamma_S)$. The results illustrate that a higher depth d does not necessarily lead to better performance. A small number of samples can still yield sufficiently accurate approximations by selecting an appropriate depth.

terms, electron correlation, and pairing mechanisms. They appear in models like quantum chemistry Hamiltonians, generalized Hubbard models, spin chain models, etc [23–26].

The required circuit depth depends on the interaction distance d_{int} of γ_S, $d_{\mathrm{int}}(S) := \max\{\,|i_{j+1}-i_j| \mid i_j \in S,\, j \in [2n-1]\,\}$. Recall Eq. (2) that the elements in S are a monotonically increasing sequence. Thus, the d_{int} could be interpreted as the maximum distance between adjacent elements in S. We prove that a random measurement circuit $\mathcal{U}_{Q_d}$ with $d = \Theta(\mathrm{polylog}\, n)$ is sufficient to make $\alpha_{S,d}$ as large as $\mathcal{O}(1/\mathrm{poly}(n))$ if $d_{\mathrm{int}} = \mathcal{O}(\log n)$ and cardinality k is a constant. From Eq. (13) and Eq. (14), we conclude that the value of $\alpha_{S,d}$ is the sum of probabilities associated with specific sites after the random walk. When the distance of the near neighborhood $i_k, i_{k+1} \in S$ logarithmically small $|i_k - i_{k+1}| = \mathcal{O}(\log(n))$, a logarithmically transition steps can traverse from $|\gamma_S, \gamma_S\rangle\rangle$ to specific sites. Due to Eq. (14), each step introduces a constant probability factor. Thus, the probability of reaching specific sites is $\mathcal{O}(1/\mathrm{poly}(n))$ after logarithmic steps random walk. We put the proof details in Appendix H.

We propose a general formula for approximating $\alpha_{S,d}$. The proposed formula considers the random walk for computing $\alpha_{S,d}$ as the several independent $k = 1$ random walks. Any two elements $i, j \in S$ are treated as an independent random walk starting from $\gamma_i\gamma_j$. After the overall random walk, the probability of $|\gamma_S, \gamma_S\rangle\rangle$ being at a specific site equals the product of the probabilities of each 1-RDM γ'_S at that site. As a result, the sum of probabilities at these specific sites can be expressed as a production $\prod \alpha_{\{i,j\},d}$. Therefore, we consider the overall random walk as the superposition of all such production

$$\alpha'_{S,d} = \frac{1}{(2k-1)!!}\left(\frac{3n}{2}\right)^k \frac{\binom{n}{k}}{\binom{2n}{2k}} \sum_{\Lambda\in \mathrm{Par}(S)} \prod_{(i,j)\in\Lambda} \alpha^L_{\{i,j\},d}, \tag{21}$$

where $\mathrm{Par}(S)$ is the set whose elements Λ are sets representing pairwise partitions of S. For example, let $S = \{1,2,3,4\}$, then $\Lambda = \{(1,2),(3,4)\}$ is a pairwise partitions of S.

Numerical experiments show that the proposed expression $\alpha'_{S,d}$ fits the true $\alpha_{S,d}$ well. Therefore, it can be concluded that $\alpha'_{S,d}$ provides a good approximation of $\alpha_{S,d}$. Fig. 1(b) show the results of comparison between $\alpha'_{S,d}$ and $\alpha_{S,d}$. The curve of $\alpha'_{S,d}$ is very close to the $\alpha_{S,d}$ when $d > 2\log(n)$, which suggests that the $\alpha'_{S,d}$ is a good approximation of $\alpha_{S,d}$ as well.

We adaptively select the depth based on the interaction distance d_{int} of a fermionic Hamiltonian H, where $d_{\mathrm{int}}(H)$ is the maximum value of $d_{\mathrm{int}}(S)$ for terms γ_S in H. Similar to the case with $|S| = 2$, we adaptive select the depth d^* as

$$d^* = \Theta\left(\max\left\{\frac{d_{\mathrm{int}}(S)^2}{\log(n)}, d_{\mathrm{int}}(S)\right\}\right). \tag{22}$$

Such d^* ensures that each term in Eq. (21) scales polynomially, thereby guaranteeing the overall $\alpha'_{S,d}$ also scales polynomially.

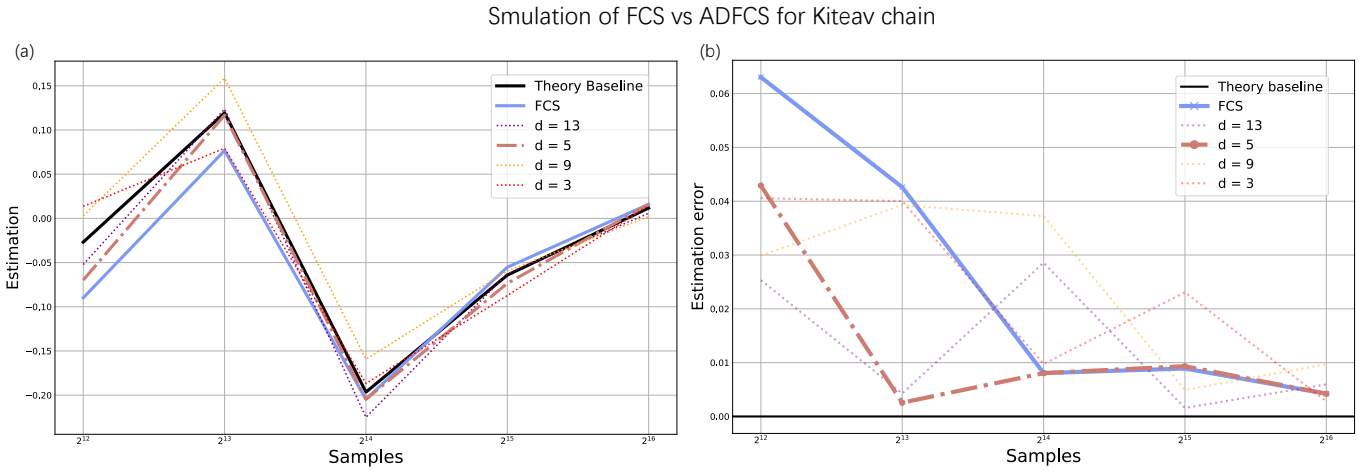

FIG. 4: Application of ADFCS to the Kitaev chain Hamiltonian H_K. (a) shows the estimation of FCS and ADFCS with varying circuit depths. All estimation align closely with the theoretical baseline. For each experiment, we set the sample numbers and randomly choose a initial state. (b) highlight the error between the estimation and the theoretical baseline. Given that the interaction distance of the Kitaev chain Hamiltonian H_K is 3, a random matchgate circuit with $d = 5$ is sufficient to achieve a good estimation of H_K.

IV. NUMERICAL EXPERIMENT

We select several typical observables γ_S and applied the ADFCS method to estimate their expected values for random 10-qubit quantum states ρ. Specifically, we investigate observables γ_S such that $|S| = 2$ with the largest and smallest interaction distances and consider cases where the set S is arranged uniformly and randomly. We use a random matchgate circuit with different depths d to measure the state ρ. The estimator is generated by R number of measurements. The absolute error between the estimator $\frac{1}{R}\sum_i \mathrm{Tr}(\hat{\rho}_i\gamma_S)$ is shown in Fig. 3. The required depth of the random matchgate circuit for a specific observable γ_S depends on the value of $\alpha_{S,d}$. When the interaction distance is small, shallower circuits tend to perform better. For instance, when $S = \{10, 11\}$, $S = [20]$, or $S = \{2, 6, 9, 10, 11, 12, 15, 16\}$, a random matchgate circuit with depth $d = 5$ provides a good estimate of the expectation value. However, when the interaction distance is larger, such as in the case of $S = \{1, 20\}$, circuits with depths ranging from $d = 15$ to $d = 23$ are required to achieve accurate expectation value estimation. If the circuit depth is chosen appropriately, a good estimate can be obtained with a relatively small number of samples.

To further test the performance of ADFCS, we apply the method of estimating the expectation of the Kiteav chain Hamiltonian. The Kitaev chain Hamiltonian is a one-dimensional model that describes a topological superconductor featuring Majorana fermions at its ends [27]. The Kiteav chain Hamiltonian is given by

$$H_K = -\frac{\mathrm{i}\mu}{2}\sum_{j=1}^{n}\gamma_{2j-1}\gamma_{2j} + \frac{\mathrm{i}}{2}\sum_{j=1}^{n-1}\left(\omega_+\gamma_{2j-1}\gamma_{2j+2} - \omega_-\gamma_{2j}\gamma_{2j+1}\right), \tag{23}$$

where μ is the chemical potential, $\omega_\pm = |\Delta| \pm t$, both Δ and $\mathcal{T}$ are certain energy gaps. We initialize a random state for 12-qubit, set these parameters as $\mu = 2$, $\Delta = 1$, and $t = 0.4$. The results are shown in Fig. 4. Since the maximum interaction distance of H_K is 3, all curves align with the theoretical values due to the short interaction distance in the insect plot. Among these curves, we highlight the curve with $d = 5$, which gives the best estimation.

V. CONCLUSION AND DISCUSSION

Estimating the expectation value of fermionic observables is a fundamental task in quantum physics and chemistry. The fermionic classical shadow method provides an innovative approach to address this problem without requiring the conversion of observables into the Pauli-basis representation. This significantly reduces the number of quantum states for certain local fermionic observables. However, the approach requires polynomial-size quantum circuits when sampling matchgate elements from $\mathbb{M}_n$ without considering the information from the fermionic observables. This imposes a considerable challenge for near-term quantum devices.

We propose an adaptive depth fermionic classical shadow (ADFCS) protocol to reduce the heavy circuit depth associated with random matchgate circuits. Using a tensor network approach, we calculate the variance for any d-depth ADFCS protocol, enabling us to determine the required depth d to ensure efficient sampling.

Furthermore, we theoretically analyze the explicit relationship between the variance and the depth d of the random matchgate circuit. Specifically, under certain assumptions, we find that the optimal depth is linear to $\max\left\{\frac{d^2_{\mathrm{int}(S)}}{\log n}, d_{\mathrm{int}(S)}\right\}$ for a given Majorana string γ_S. Numerical fitting results are also provided to support our theoretical findings.

We validate the correctness of our algorithm by evaluating the expectation values of several Majorana strings with respect to randomly generated quantum states ρ. The numerical results align with and support our theoretical findings. Additionally, we applied our algorithm to estimate the expectation value of a Kitaev chain Hamiltonian. Comparative numerical analysis demonstrates that our ADFCS algorithm achieves performance comparable to the FCS algorithm, while requiring a significantly shallower circuit depth.

ACKNOWLEDGEMENTS

[1] Alán Aspuru-Guzik, Anthony D Dutoi, Peter J Love, and Martin Head-Gordon. Simulated quantum computation of molecular energies. *Science*, 309(5741):1704–1707, 2005.

[2] Yudong Cao, Jonathan Romero, Jonathan P Olson, Matthias Degroote, Peter D Johnson, Mária Kieferová, Ian D Kivlichan, Tim Menke, Borja Peropadre, Nicolas PD Sawaya, et al. Quantum chemistry in the age of quantum computing. *Chemical reviews*, 119(19):10856–10915, 2019.

[3] Hsin-Yuan Huang, Richard Kueng, and John Preskill. Predicting many properties of a quantum system from very few measurements. *Nature Physics*, 16(10):1050–1057, 2020.

[4] Andrew Zhao, Nicholas C. Rubin, and Akimasa Miyake. Fermionic partial tomography via classical shadows. *Phys. Rev. Lett.*, 127:110504, Sep 2021.

[5] Guang Hao Low. Classical shadows of fermions with particle number symmetry. *arXiv preprint arXiv:2208.08964*, 2022.

[6] Kianna Wan, William J. Huggins, Joonho Lee, and Ryan Babbush. Matchgate shadows for fermionic quantum simulation, 2022.

[7] Ketan N Patel, Igor L Markov, and John P Hayes. Optimal synthesis of linear reversible circuits. *Quantum Inf. Comput.*, 8(3):282–294, 2008.

[8] Jiaqing Jiang, Xiaoming Sun, Shang-Hua Teng, Bujiao Wu, Kewen Wu, and Jialin Zhang. Optimal space-depth trade-off of cnot circuits in quantum logic synthesis. In *Proceedings of the Fourteenth Annual ACM-SIAM Symposium on Discrete Algorithms*, pages 213–229. SIAM, 2020.

[9] Zhang Jiang, Kevin J Sung, Kostyantyn Kechedzhi, Vadim N Smelyanskiy, and Sergio Boixo. Quantum algorithms to simulate many-body physics of correlated fermions. *Physical Review Applied*, 9(4):044036, 2018.

[10] Frank Arute, Kunal Arya, Ryan Babbush, Dave Bacon, Joseph C Bardin, Rami Barends, Rupak Biswas, Sergio Boixo, Fernando GSL Brandao, David A Buell, et al. Quantum supremacy using a programmable superconducting processor. *Nature*, 574(7779):505–510, 2019.

[11] Yulin Wu, Wan-Su Bao, Sirui Cao, Fusheng Chen, Ming-Cheng Chen, Xiawei Chen, Tung-Hsun Chung, Hui Deng, Yajie Du, Daojin Fan, Ming Gong, Cheng Guo, Chu Guo, Shaojun Guo, Lianchen Han, Linyin Hong, He-Liang Huang, Yong-Heng Huo, Liping Li, Na Li, Shaowei Li, Yuan Li, Futian Liang, Chun Lin, Jin Lin, Haoran Qian, Dan Qiao, Hao Rong, Hong Su, Lihua Sun, Liangyuan Wang, Shiyu Wang, Dachao Wu, Yu Xu, Kai Yan, Weifeng Yang, Yang Yang, Yangsen Ye, Jianghan Yin, Chong Ying, Jiale Yu, Chen Zha, Cha Zhang, Haibin Zhang, Kaili Zhang, Yiming Zhang, Han Zhao, Youwei Zhao, Liang Zhou, Qingling Zhu, Chao-Yang Lu, Cheng-Zhi Peng, Xiaobo Zhu, and Jian-Wei Pan. Strong quantum computational advantage using a superconducting quantum processor. *Phys. Rev. Lett.*, 127:180501, Oct 2021.

[12] Sirui Cao, Bujiao Wu, Fusheng Chen, Ming Gong, Yulin Wu, Yangsen Ye, Chen Zha, Haoran Qian, Chong Ying, Shaojun Guo, et al. Generation of genuine entanglement up to 51 superconducting qubits. *Nature*, 619(7971):738–742, 2023.

[13] Christian Bertoni, Jonas Haferkamp, Marcel Hinsche, Marios Ioannou, Jens Eisert, and Hakop Pashayan. Shallow shadows: Expectation estimation using low-depth random clifford circuits. *Physical Review Letters*, 133(2):020602, 2024.

[14] Thomas Schuster, Jonas Haferkamp, and Hsin-Yuan Huang. Random unitaries in extremely low depth. *arXiv preprint arXiv:2407.07754*, 2024.

[15] Pierre-Gabriel Rozon, Ning Bao, and Kartiek Agarwal. Optimal twirling depth for classical shadows in the presence of noise. *Phys. Rev. Lett.*, 133:130803, Sep 2024.

[16] Robbie King, David Gosset, Robin Kothari, and Ryan Babbush. Triply efficient shadow tomography. *arXiv preprint arXiv:2404.19211*, 2024.

[17] Lucas Hackl and Eugenio Bianchi. Bosonic and fermionic gaussian states from kähler structures. *SciPost Physics Core*, 4(3):025, 2021.

[18] Leslie G. Valiant. Quantum circuits that can be simulated classically in polynomial time. *SIAM Journal on Computing*, 31(4):1229–1254, 2002.
[19] Senrui Chen, Wenjun Yu, Pei Zeng, and Steven T. Flammia. Robust shadow estimation. *PRX Quantum*, 2:030348, Sep 2021.
[20] Ari M. Turner, Frank Pollmann, and Erez Berg. Topological phases of one-dimensional fermions: An entanglement point of view. *Phys. Rev. B*, 83:075102, Feb 2011.
[21] Luca Giuggioli. Exact spatiotemporal dynamics of confined lattice random walks in arbitrary dimensions: a century after smoluchowski and pólya. *Physical Review X*, 10(2):021045, 2020.
[22] Gregory F Lawler and Vlada Limic. *Random walk: a modern introduction*, volume 123. Cambridge University Press, 2010.
[23] James D Whitfield, Jacob Biamonte, and Alán Aspuru-Guzik. Simulation of electronic structure hamiltonians using quantum computers. *Molecular Physics*, 109(5):735–750, 2011.
[24] Assa Auerbach. *Interacting electrons and quantum magnetism*. Springer Science & Business Media, 2012.
[25] Qimiao Si and J Lleweilun Smith. Kosterlitz-thouless transition and short range spatial correlations in an extended hubbard model. *Physical review letters*, 77(16):3391, 1996.
[26] Elliott Lieb, Theodore Schultz, and Daniel Mattis. Two soluble models of an antiferromagnetic chain. *Annals of Physics*, 16(3):407–466, 1961.
[27] A Yu Kitaev. Unpaired majorana fermions in quantum wires. *Physics-uspekhi*, 44(10S):131, 2001.

Appendix A: Introduction to Pauli-transfer matrix representation

By employing the Jordan-Wigner transformation, we can express γ_S in terms of Pauli operators. The Pauli-transfer matrix (PTM) representation uses these Pauli operators $\{\sigma_i\}_{i=1}^{2^n}$ as a basis, where $\sigma_i = P_i/\sqrt{2^n}$ is the normalized Pauli operator, allowing us to denote the non-zero linear operators A as a 4^n-length vector $|A\rangle\rangle$ with the j-th entry being

$$A_j = \mathrm{Tr}(A\sigma_j). \tag{A1}$$

In this representation, a channel of operators could be expressed as a matrix Λ with the (a,b)-th element being

$$\Lambda(a,b) = \mathrm{Tr}(\sigma_b \Lambda(\sigma_a)). \tag{A2}$$

Using this expression, we can represent the second moment of the random matchgate as a fourth-order tensor, which is shown in Appendix D.

Appendix B: Majorana operators could diagonalize shadow channel

This section shows the details about diagonalizing shadow channel $\mathcal{M}_d$. Notice that the computational basis $|b\rangle$ are Gaussian states

$$|b\rangle\langle b| = \prod_{j=1}^{n} \frac{1}{2}\left(I - \mathrm{i}(-1)^{b_j}\gamma_{2j-1}\gamma_{2j}\right). \tag{B1}$$

Thus, any basis $|b\rangle\langle b|$ can be prepared from the state $|b\rangle\langle b|$ by a Gaussian unitary $U_Q \in \mathbb{M}_n$, which indicates that Pauli-X is in the matchgate group. The state $|b\rangle = |b_1 b_2 \cdots b_n\rangle$ could be denoted as $\prod X_i^{b_i}|0\rangle$. Since Pauli-X is in the matchgate group, we can absorb the $\prod X_{b_i}$ into the matchgates U_{Q_d} in the expression of shadow channel

$$\mathcal{M}_d(\gamma_S) = \int \mathrm{d}U_{Q_d} \sum_{b\in\{0,1\}^n} \langle b| U_{Q_d}\gamma_S U_{Q_d}^\dagger |b\rangle U_{Q_d}^\dagger |b\rangle \langle b| U_{Q_d} \tag{B2}$$

$$= 2^n \int \mathrm{d}U_{Q_d} \langle 0| U_{Q_d}\gamma_S U_{Q_d}^\dagger |0\rangle U_{Q_d}^\dagger |0\rangle \langle 0| U_{Q_d}. \tag{B3}$$

If S' is not equal to S and the layer number d is not equal to zero, then there exists a permutation matrix Q'_d in one depth matchgate circuit such that

$$[\gamma_S, U_{Q'_d}] = 0, \quad \{\gamma_{S'}, U_{Q'_d}\} = 0. \tag{B4}$$

The Q'_d could be constructed in one depth because such U'_{Q_d} could be a Pauli operator, which involves one depth matchgate circuit. It implies

$$\frac{1}{2^n}\mathrm{Tr}\left(\gamma_{S'}\mathcal{M}_d(\gamma_S)\right) = \int \mathrm{d}U_{Q_d} \left\langle 0\right| U_{Q_d}\gamma_S U_{Q_d}^\dagger \left|0\right\rangle \left\langle 0\right| U_Q \gamma_{S'} U_{Q_d}^\dagger \left|0\right\rangle \tag{B5}$$

$$= \int \mathrm{d}U_{Q_d} \left\langle 0\right| U_{Q_d} U_{Q'_d}\gamma_S U_{Q'_d}^\dagger U_{Q_d}^\dagger \left|0\right\rangle \left\langle 0\right| U_{Q_d} U_{Q'_d}\gamma_{S'} U_{Q'_d}^\dagger U_{Q_d}^\dagger \left|0\right\rangle \tag{B6}$$

$$= -\int \mathrm{d}U_{Q_d} \left\langle 0\right| U_{Q_d}\gamma_S U_{Q_d}^\dagger \left|0\right\rangle \left\langle 0\right| U_{Q_d} \gamma_{S'} U_{Q_d}^\dagger \left|0\right\rangle . \tag{B7}$$

The result shows that $\mathrm{Tr}\left(\gamma_{S'}\mathcal{M}_d(\gamma_S)\right) = 0$ when S' is not equal to S, thereby $\mathcal{M}_d(\gamma_S) = \alpha_{s,d}\gamma_S$.

Appendix C: Bound the variance of ADFCS estimator with $\alpha_{S,d}$

The variance of the random variable $v = \mathrm{Tr}(\hat{\rho}\gamma_S)$ is analyzed by deriving an upper bound on its value. First, the variance is bounded by the expected squared magnitude of v, i.e., $\mathrm{Var}[v] \leq \mathbb{E}[|v|^2]$. The expectation is then expressed as an integral over the unitary group U_{Q_d} and averaged over the state ρ

$$\mathbb{E}[|v|^2] = \int \mathrm{d}U_{Q_d}\, \mathbb{E}_\rho \left[\sum_b \langle b|U_{Q_d}\rho U_{Q_d}^\dagger|b\rangle \left|\langle b|U_{Q_d}\mathcal{M}_d^{-1}(\gamma_S)U_{Q_d}^\dagger|b\rangle\right|^2\right]. \tag{C1}$$

Now, we start to simplify the expression. Firstly, we average out the ρ, which leads to

$$\mathbb{E}[|v|^2] = 2^{-n}\int \mathrm{d}U_{Q_d} \sum_b \left|\langle b|U_{Q_d}\mathcal{M}_d^{-1}(\gamma_S)U_{Q_d}^\dagger|b\rangle\right|^2. \tag{C2}$$

Next, we denote $|b\rangle$ as $\prod_i X_i^{b_i}|0\rangle$ and absorb the Pauli X operators into the matchgate operators. And then uses Eq. (8)

$$\mathbb{E}[|v|^2] = \frac{1}{|\alpha_{S,d}|^2}\int \langle 0|U_{Q_d}\gamma_S U_{Q_d}^\dagger|0\rangle\langle 0|U_{Q_d}\gamma_S^\dagger U_{Q_d}^\dagger|0\rangle \tag{C3}$$

$$= \frac{1}{\alpha_{S,d}}. \tag{C4}$$

Finally we have $\mathrm{Var}[v] \leq \frac{1}{\alpha_{S,d}}$. Notice that this inequality can be easily taken equally when $\mathrm{Tr}\left(\rho\gamma_S\right) = 0$. Therefore the order of $\alpha_{S,d}$ determines the order of variance, thereby determining the sample complexity.

Appendix D: Details of simplifying $\alpha_{S,d}$ to tensore network

This section shows the details of representing $\alpha_{S,d}$ by the tensor network contraction in PTM representation. According to Lemma 2, the $\alpha_{S,d}$ could be expressed by

$$\alpha_{S,d} = 2^{2n}\langle\langle \mathbf{0},\mathbf{0}| \int \mathrm{d}U_{Q_d}\mathcal{U}_{Q_d}^{\otimes 2}|P_S,P_S\rangle\rangle, \tag{D1}$$

where P_S is the Pauli string corresponding to γ_S via Jordan-Wigner transformation.

Since each two-qubit random matchgate is independently sampled, the integral $\int \mathrm{d}U_Q\mathcal{U}_Q^{\otimes 2}$ could be calculated by independently integrating each 2-qubit matchgate. The result of the integral of the 2-qubit matchgates is given by

T	II	IX	IY	IZ	XI	XX	XY	XZ	YI	YX	YY	YZ	ZI	ZX	ZY	ZZ
II	1															
IX		1/4	1/4					1/4				1/4				
IY		1/4	1/4					1/4				1/4				
IZ				1/6		1/6	1/6			1/6	1/6		1/6			
XI					1/4				1/4					1/4	1/4	
XX				1/6		1/6	1/6			1/6	1/6		1/6			
XY				1/6		1/6	1/6			1/6	1/6		1/6			
XZ		1/4	1/4					1/4				1/4				
YI					1/4				1/4					1/4	1/4	
YX				1/6		1/6	1/6			1/6	1/6		1/6			
YY				1/6		1/6	1/6			1/6	1/6		1/6			
YZ		1/4	1/4					1/4				1/4				
ZI				1/6		1/6	1/6			1/6	1/6		1/6			
ZX					1/4				1/4					1/4	1/4	
ZY					1/4				1/4					1/4	1/4	
ZZ																1

TABLE I: Values of tensor $\mathcal{T}$. The head of columns represents the input of $\mathcal{T}$ while the head of rows represents the output of $\mathcal{T}$. For example, the values in row 'XY' and column 'YZ' represent the value T^{XY}_{YZ}. The blank space of the table stands for 0. For example, T^{XY}_{YZ} is equal to $\frac{1}{6}$.

Lemma 1,

$$\begin{aligned}\int_{U_Q\sim\mathbb{M}_2} \mathrm{d}U_Q \mathcal{U}_Q^{\otimes 2} =& |\gamma_\emptyset\rangle\rangle|\gamma_\emptyset\rangle\rangle\langle\langle\gamma_\emptyset|\langle\langle\gamma_\emptyset| + \frac{1}{4}\sum_{i,j}|\gamma_i\rangle\rangle|\gamma_i\rangle\rangle\langle\langle\gamma_j|\langle\langle\gamma_j| \\ &+ \frac{1}{6}\sum_{\substack{i_1\neq i_2\\ j_1\neq j_2}}|\gamma_{i_1}\gamma_{i_2}\rangle\rangle|\gamma_{i_1}\gamma_{i_2}\rangle\rangle\langle\langle\gamma_{j_1}\gamma_{j_2}|\langle\langle\gamma_{j_1}\gamma_{j_2}| \\ &+ \frac{1}{4}\sum_{\substack{i_1\neq i_2, j_1\neq j_2\\ i_1\neq i_3, j_1\neq j_3\\ i_2\neq i_3, j_2\neq j_3}}|\gamma_{i_1}\gamma_{i_2}\gamma_{i_3}\rangle\rangle|\gamma_{i_1}\gamma_{i_2}\gamma_{i_3}\rangle\rangle\langle\langle\gamma_{j_1}\gamma_{j_2}\gamma_{j_3}|\langle\langle\gamma_{j_1}\gamma_{j_2}\gamma_{j_3}| \\ &+ |\gamma_1\gamma_2\gamma_3\gamma_4\rangle\rangle|\gamma_1\gamma_2\gamma_3\gamma_4\rangle\rangle\langle\langle\gamma_1\gamma_2\gamma_3\gamma_4|\langle\langle\gamma_1\gamma_2\gamma_3\gamma_4|,\end{aligned} \tag{D2}$$

where i, j are index ranged from 1 to 4. Follow the definition Equation (12), each element of tensor $\mathcal{T}$ could be calculated by Eq. (D2). We show these concrete elements in Table I. The tensor $\mathcal{T}$ presents the average effect of a random two-qubit matchgate.

Here, we represented $|\mathbf{0},\mathbf{0}\rangle\rangle$ in PTM to complete the calculation $\alpha_{S,d} = \langle\langle\mathbf{0},\mathbf{0}|\mathcal{C}|\gamma_S,\gamma_S\rangle\rangle$. Notice the matrix identity

$$|\mathbf{0}\rangle\langle\mathbf{0}| = \frac{1}{2^n}\sum_{\Lambda\subset[2n]}\prod_{i\in\Lambda} Z_i, \tag{D3}$$

where Z_i denotes the application of the Pauli Z operator to the i-th qubit. Especially, when $\Lambda=\emptyset$, let $\prod_{i\in\Lambda} Z_i = \mathbb{1}_n$. Then, the super vector of $|\mathbf{0},\mathbf{0}\rangle\rangle$ could be expressed as

$$|\mathbf{0},\mathbf{0}\rangle\rangle = \frac{1}{2^{2n}}\sum_{\Lambda,\Lambda'\subset[2n]}|\prod_{i\in\Lambda} Z_i, \prod_{j\in\Lambda'} Z_j\rangle\rangle. \tag{D4}$$

Eq. (D4) express the supervector $|\mathbf{0},\mathbf{0}\rangle\rangle$ in the PTM representation. Finally, we write the $\mathcal{C}$, $|\mathbf{0},\mathbf{0}\rangle\rangle$, and $|\gamma_S,\gamma_S\rangle\rangle$ in Pauli basis. Thus, the $\alpha_{S,d}$ calculation could be expressed as the tensor network contraction, as illustrated in Fig. 2.

Lemma 2. *The $\alpha_{S,d}$ obey the identity $\alpha_{S,d} = 2^{2n}\langle\langle\mathbf{0},\mathbf{0}|\int \mathrm{d}U_{Q_d}\mathcal{U}_{Q_d}^{\otimes 2}|P_S,P_S\rangle\rangle$, where P_S is the Pauli string corresponding to γ_S via Jordan-Wigner transformation.*

Proof. Follow the definition of $\alpha_{S,d}$, we have

$$\alpha_{S,d} = \int_{Q\sim O_d} \mathrm{d}U_{Q_d} \left| \langle \mathbf{0}| U_{Q_d} \gamma_S U_{Q_d}^\dagger |\mathbf{0}\rangle \right|^2 \tag{D5}$$

$$= \int_{Q\sim O_d} \mathrm{d}U_{Q_d} \langle \mathbf{0}| U_{Q_d} \gamma_S U_{Q_d}^\dagger |\mathbf{0}\rangle \langle \mathbf{0}| U_{Q_d} \gamma_S^\dagger U_{Q_d}^\dagger |\mathbf{0}\rangle . \tag{D6}$$

The subscript d denotes the layer number of the matchgate circuit. The expression could be simplified by substituting the relationship between $\gamma_S^\dagger$ and γ_S, which is

$$\gamma_S^\dagger = (-1)^{\frac{|S|(|S|-1)}{2}} \gamma_S. \tag{D7}$$

The relation is true because of the anti-commutation relation of Majorana operators $\{\gamma_i, \gamma_j\} = 2\delta_{ij}$. The anti-commutation relation produces a coefficient of $(-1)^{|S|-1}$ when γ_{l_1} is moved to the first place. Then, the $\gamma_S^\dagger$ could be calculated by

$$\gamma_S^\dagger = (-1)^{|S|-1} \gamma_{l_1} \gamma_{l_{|S|}} \gamma_{l_{|S|-1}} \cdots \gamma_{l_2} \tag{D8}$$

$$= (-1)^{|S|-1+|S|-2} \gamma_{l_1} \gamma_{l_2} \gamma_{l_{|S|}} \gamma_{l_{|S|-1}} \cdots \gamma_{l_3} \tag{D9}$$

$$= (-1)^{\frac{|S|(|S|-1)}{2}} \gamma_S. \tag{D10}$$

By substituting Eq. (D10), the $\alpha_{S,d}$ could be expressed as

$$\alpha_{S,d} = (-1)^{\frac{|S|(|S|-1)}{2}} \int \mathrm{d}U_{Q_d} \langle \mathbf{0}| U_{Q_d} \gamma_S U_{Q_d}^\dagger |\mathbf{0}\rangle^2 \tag{D11}$$

$$= (-1)^{\frac{|S|(|S|-1)}{2}} \int \mathrm{d}U_{Q_d} \mathrm{tr}\Big(U_{Q_d} \gamma_S U_{Q_d}^\dagger |\mathbf{0}\rangle \langle \mathbf{0}| \Big)^2 \tag{D12}$$

$$= (-1)^{\frac{|S|(|S|-1)}{2}} 2^{2n} \int \mathrm{d}U_{Q_d} \langle\langle \mathbf{0}, \mathbf{0}| \mathcal{U}_{Q_d}^{\otimes 2} |\gamma_S, \gamma_S\rangle\rangle \tag{D13}$$

$$= (-1)^{\frac{|S|(|S|-1)}{2}} 2^{2n} \langle\langle \mathbf{0}, \mathbf{0}| \int \mathrm{d}U_{Q_d} \mathcal{U}_{Q_d}^{\otimes 2} |\gamma_S, \gamma_S\rangle\rangle. \tag{D14}$$

In PTM representation, the γ_S is corresponded to a Pauli basis with a phase $\pm \mathrm{i}^{\lfloor |S|/2 \rfloor}$. Thus, the super vector $|\gamma_S, \gamma_S\rangle\rangle$ could be represented as

$$|\gamma_S, \gamma_S\rangle\rangle = (-1)^{\lfloor \frac{|S|}{2} \rfloor} |P^S, P^S\rangle\rangle, \tag{D15}$$

where P^S is the Pauli operator that corresponding to the γ_S.

Follows Eq. (D14) and Eq. (D15), the sign of $\alpha_{S,d}$ is determined by $(-1)^{\frac{|S|(|S|-1)}{2}} (-1)^{\lfloor |S|/2 \rfloor}$. We show that the sign equals to 1 by categorizing the parity of $|S|$.

1. $|S|$ **is an odd number.** Let $|S| = 2q+1$, $q \in \mathbb{N}$, $q \geq 0$. And then

$$(-1)^{\frac{|S|(|S|-1)}{2}} (-1)^{\lfloor |S|/2 \rfloor} = (-1)^{q(2q+1)+q} = 1. \tag{D16}$$

2. $|S|$ **is an even number.** Let $|S| = 2q$, $q \in \mathbb{N}$, $q \geq 0$. And then

$$(-1)^{\frac{|S|(|S|-1)}{2}} (-1)^{\lfloor |S|/2 \rfloor} = (-1)^{(2q-1)q+q} = 1. \tag{D17}$$

Thus, we conclude that the $\alpha_{S,d}$ could be expressed by

$$\alpha_{S,d} = (-1)^{\frac{|S|(|S|-1)}{2}} (-1)^{\lfloor |S|/2 \rfloor} 2^{2n} \langle\langle \mathbf{0}, \mathbf{0}| \int \mathrm{d}U_{Q_d} \mathcal{U}_{Q_d}^{\otimes 2} |P_S, P_S\rangle\rangle \tag{D18}$$

$$= \langle\langle \mathbf{0}, \mathbf{0}| \int \mathrm{d}U_{Q_d} \mathcal{U}_{Q_d}^{\otimes 2} |P_S, P_S\rangle\rangle. \tag{D19}$$

□

Appendix E: Mapping the action of tensors to random walk

Here, we give some notations to express the properties of the $\alpha_{S,d}$ tensor network. Let $\mathcal{T}^{(o)}$ represent the odd layer of $\mathcal{T}$ tensors, and $\mathcal{T}^{(e)}$ represent the even layer of $\mathcal{T}$ tensors. Any tensor network $\mathcal{C}$ with brickwork architecture could be expressed by alternately apply $\mathcal{T}^{(o)}$ and $\mathcal{T}^{(e)}$ gates,

$$\mathcal{C}\left(t, b_1, b_2\right) = {\mathcal{T}^{(o)}}^{b_2} \mathcal{B}^t {\mathcal{T}^{(e)}}^{b_1}, \tag{E1}$$

where $b_1, b_2 \in \{0, 1\}$, $t + b_1 + b_2$ stands for the number of layers, and $\mathcal{B} = \mathcal{T}^{(e)}\mathcal{T}^{(o)}$. Let Γ_n' denote the vectorized double supervector space of Γ_n, defined as $\Gamma_n' = \mathrm{span}\{|\gamma_S, \gamma_S\rangle\rangle \mid \gamma_S \in \Gamma_n\}$. Notably, both $\mathcal{T}^{(o)}$ and $\mathcal{T}^{(e)}$ gates are projection operators, satisfying $(\mathcal{T}^{(e)})^2 = \mathcal{T}^{(e)}$ and $(\mathcal{T}^{(o)})^2 = \mathcal{T}^{(o)}$.

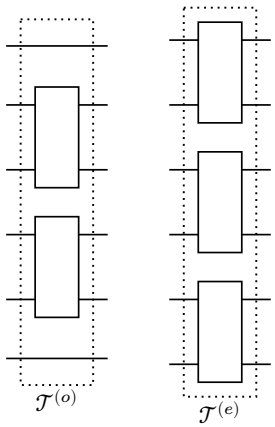

In the main text, we frequently use the word "representation" but avoid the rigorous description of it. Here, we use the language of representation theory to give a description of representing $\mathcal{C}$ in mathematical taste. As we mentioned in the main text, the whole tensor $\mathcal{C}$ could be expressed by

$$\mathcal{C} = \begin{cases} \mathcal{B}^t, & d = 2t \\ \mathcal{B}^t \mathcal{T}_{\mathrm{init}}, & d = 2t + 1. \end{cases} \tag{E2}$$

For odd depth cases, studying the contraction of $\mathcal{C}$ on Γ_n' is equivalent to analyzing the action of the group $\{\mathcal{B}^t\}$ on the representation space $\mathcal{T}_{\mathrm{init}}(\Gamma_n')$. The situation is similar for the even depth cases when $t \geq 1$. The difference between the two cases is the initial state, which is $\mathcal{T}^{(e)}|\gamma_S, \gamma_S\rangle\rangle$ for even depth case, and $\mathcal{T}^{(e)}\mathcal{T}^{(o)}|\gamma_S, \gamma_S\rangle\rangle$ for odd depth case. The states $\mathcal{T}^{(e)}\mathcal{T}^{(o)}|\gamma_S, \gamma_S\rangle\rangle$ are still in the space $\mathcal{T}_{\mathrm{init}}(\Gamma_n')$, thereby we can apply similar method on the even depth cases. Thus, whatever the depth is even or odd, the contraction of $\mathcal{C}$ on Γ_n' could be analyzed by studying the representation of group $\{\mathcal{B}^t\}$. We use the word "the representation of $\mathcal{C}$" for short.

To simplify the analysis, we analyze the random circuit with even qubit number and odd depth d. We will represent $\mathcal{C}$ for the γ_S with $|S| = 2$ in polynomial space, as illustrated in Fig. 5. These conditions will be maintained throughout the remainder of this section to ensure consistency and clarity in the discussion.

1. Reduce the calculation to polynomial space

We represent $\mathcal{C}|\gamma_S, \gamma_S\rangle\rangle$ using polynomial space because it provides the essential properties we require, such as multiplication and addition, which will be important for further analysis.

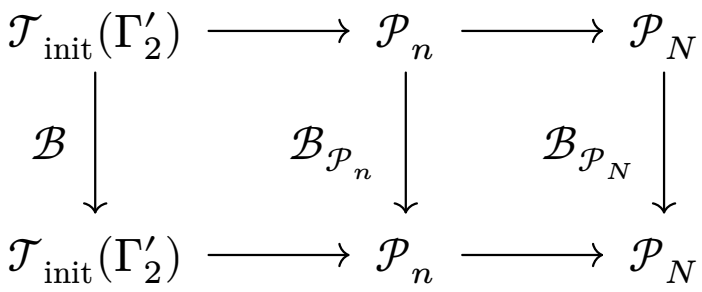

FIG. 5: The diagram shows how we simplify the calculation step by step. Γ_2' is the vectorized double supervector space. The horizontal arrows point from one space to another space. The vertical arrows represent the corresponding operators of $\mathcal{B}$ within different representations. Finally, we reduce it to the N-elementary polynomial of the 2nd degree polynomial space.

According to Table I, $\mathcal{T}_{\text{init}}(\Gamma_2')$ could be spanned by the operators with the following form

$$\begin{cases} |\psi_{ij}\rangle\rangle = & \frac{1}{4}|X_i\left(\prod_{k=i+1}^{j-1} Z_k\right)Y_j\rangle\rangle^{\otimes 2} + \frac{1}{4}|X_i\left(\prod_{k=i+1}^{j-1} Z_k\right)Y_j\rangle\rangle^{\otimes 2} \\ & +\frac{1}{4}|X_i\left(\prod_{k=i+1}^{j-1} Z_k\right)Y_j\rangle\rangle^{\otimes 2} + \frac{1}{4}|X_i\left(\prod_{k=i+1}^{j-1} Z_k\right)Y_j\rangle\rangle^{\otimes 2},\ i<j \\ |\psi_{ii}\rangle\rangle = & |Z_i, Z_i\rangle\rangle. \end{cases} \tag{E3}$$

The isometric map $\phi : \mathcal{T}_{\text{init}}(\Gamma_2') \to \mathcal{P}_n$ could be constructed by $\phi(|\psi_{ij}\rangle\rangle) := x_i x_j$, $\phi(|\psi_{ii}\rangle\rangle) := x_i^2$. The linear map ϕ is a homomorphism with inverse, which means it is an isometric between $\mathcal{T}_{\text{init}}(\Gamma_2')$ and $\mathcal{P}_n$. The action of $\mathcal{C}$ in $\mathcal{P}_n$ is constructed by

$$\mathcal{C}_{\mathcal{P}_n}(\cdot) := \phi \circ \mathcal{C} \circ \phi^{-1}(\cdot). \tag{E4}$$

Thus, the action of d-layer matchgate circuit on the $\gamma_{\{i,j\}}$ is equivalent to the action of $\mathcal{C}_{\mathcal{P}_n}$ on the term $x_i x_j$. Due to Lemma 3, the action could be further simplified by finding a sub-representation $\mathcal{P}_N$ of representation $\mathcal{P}_n$, where N equals to $\frac{n}{2}$. Recall that n is an even number so N is an integer.

Certain hidden patterns are revealed by reducing the representation to the polynomial space $\mathcal{P}_N$. Most of the main results are been proved in the $\mathcal{P}_N$.

Lemma 3. *The space $\mathcal{P}_N$ isometric to a sub-representation of $\mathcal{P}_n$.*

Proof. Define the map φ as

$$\begin{aligned} \varphi : \mathcal{P}_N &\to \mathcal{P}_n \\ y_i^2 &\mapsto x_{2i-1}^2 + 4x_{2i-1}x_{2i} + x_{2i}^2 \\ y_i y_j &\mapsto (x_{2i-1} + x_{2i})(x_{2j-1} + x_{2j}). \end{aligned} \tag{E5}$$

We define the φ as a linear function so that the definition of mapping on a basis induces the mapping on any element of the space

$$\varphi(\sum \xi_{ij} y_i y_j) = \sum \xi_{ij} \varphi(y_i y_j). \tag{E6}$$

Thus, the space $\varphi(\mathcal{P}_N)$ is a linear subspace of $\mathcal{P}_n$. Because φ is an injection, there is a map $\varphi' : \mathcal{P}_n \to \mathcal{P}_N$ such that $\varphi' \circ \varphi$ is identity. The action of $\mathcal{C}$ in $\mathcal{P}_N$ is constructed by

$$\mathcal{C}_{\mathcal{P}_N}(y_i y_j) := \varphi' \circ \mathcal{C}_{\mathcal{P}_n} \circ \varphi(y_i y_j). \tag{E7}$$

Based on the definition of representation, the space $\mathcal{P}_N$ is a representation of $\mathcal{C}$. And Eq. (E7) depict how to act a tensor on $\mathcal{P}_N$.

The next step is to show that such a representation of $\mathcal{C}$ does not "lose information". Formally, we need to prove that the representation $\mathcal{P}_n$ could be reduced to a sub-representation isometrics to $\mathcal{P}_N$. Naturally, we will consider whether the subspace $\varphi(\mathcal{P}_N)$ will constitute a sub-representation. If it is true, we could reduce the representation to its faithful sub-representation $\varphi(\mathcal{P}_N) \subset P_n$, which isometric to the polynomial space $\varphi(\mathcal{P}_N) \simeq \mathcal{P}_N$.

By the definition of sub-representation, we need to prove

$$\mathcal{B}^t(\varphi(\mathcal{P}_N)) \subset \varphi(\mathcal{P}_N), \quad \forall t. \tag{E8}$$

The proof of statement (E8) will be carried out using mathematical induction.

When $t = 0$, $\varphi(\mathcal{P}_N) \subset \varphi(\mathcal{P}_N)$ is true. Suppose the statement is true for t^*, then we have

$$(\mathcal{T}^{(e)}_{\mathcal{P}_n}\mathcal{T}^{(o)}_{\mathcal{P}_n})^{t^*}(\varphi(y_i y_j)) = \sum \xi_{lm}\varphi(y_l y_m). \tag{E9}$$

And then

$$\begin{aligned}
\mathcal{B}^{t^*+1}_{\mathcal{P}_n}(\varphi(y_i y_j)) =& \mathcal{T}^{(e)}_{\mathcal{P}_n}\mathcal{T}^{(o)}_{\mathcal{P}_n}(\sum \xi_{lm}\varphi(y_l y_m)) && \text{(E10)}\\
=& \sum \xi_{lm}\delta_{lm}\mathcal{T}^{(e)}_{\mathcal{P}_n}\mathcal{T}^{(o)}_{\mathcal{P}_n}(x^2_{2i-1} + 4x_{2i-1}x_{2i} + x^2_{2i}) && \text{(E11)}\\
&+ \sum \xi_{lm}(1-\delta_{lm})\mathcal{T}^{(e)}_{\mathcal{P}_n}\mathcal{T}^{(o)}_{\mathcal{P}_n}\left((x_{2i-1} + x_{2i})\,(x_{2j-1} + x_{2j})\right), && \text{(E12)}
\end{aligned}$$

where $\mathcal{B}_{\mathcal{P}_n}$, $\mathcal{T}^{(e)}_{\mathcal{P}_n}$ and $\mathcal{T}^{(o)}_{\mathcal{P}_n}$ are defined in a manner analogous to $\mathcal{C}_{\mathcal{P}_n}$. We will prove Eq. (E11) is in the space $\varphi(\mathcal{P}_N)$, while the same result of Eq. (E12) can be proved by straightforward calculation

$$\begin{aligned}
&\mathcal{T}^{(e)}_{\mathcal{P}_n}\mathcal{T}^{(o)}_{\mathcal{P}_n}(x^2_{2i-1} + 4x_{2i-1}x_{2i} + x^2_{2i})\\
=&\mathcal{T}^{(e)}_{\mathcal{P}_n}(\frac{1}{6}x^2_{2i-2} + \frac{2}{3}x_{2i-2}x_{2i-1} + x_{2i-2}x_{2i} + x_{2i-2}x_{2i+1}\\
&+ \frac{1}{6}x^2_{2i-1} + x_{2i-1}x_{2i} + x_{2i-1}x_{2i+1}\\
&+ \frac{1}{6}x^2_{2i} + \frac{2}{3}x_{2i}x_{2i+1} + \frac{1}{6}x^2_{2i+1})\\
=&\frac{1}{36}x^2_{2i-3} + \frac{1}{9}x_{2i-3}x_{2i-2} + \frac{5}{12}x_{2i-3}x_{2i-1} + \frac{5}{12}x_{2i-3}x_{2i} + \frac{1}{4}x_{2i-3}x_{2i+1} + \frac{1}{4}x_{2i-3}x_{2i+2}\\
&+ \frac{1}{36}x^2_{2i-2} + \frac{5}{12}x_{2i-2}x_{2i-1} + \frac{5}{12}x_{2i-2}x_{2i} + \frac{1}{4}x_{2i-2}x_{2i+1} + \frac{1}{4}x_{2i-2}x_{2i+2}\\
&+ \frac{2}{9}x^2_{2i-1} + \frac{8}{9}x_{2i-1}x_{2i} + \frac{5}{12}x_{2i-1}x_{2i+1} + \frac{5}{12}x_{2i-1}x_{2i+2}\\
&+ \frac{2}{9}x^2_{2i} + \frac{5}{12}x_{2i}x_{2i+1} + \frac{5}{12}x_{2i}x_{2i+2}\\
&+ \frac{1}{36}x^2_{2i+1} + \frac{1}{9}x_{2i+1}x_{2i+2}\\
&+ \frac{1}{36}x^2_{2i+2}
\end{aligned} \tag{E13}$$

The result expression is in $\varphi(\mathcal{P}_N)$ because we could find a polynomial y in $\mathcal{P}_N$ such that $\varphi(y)$ equals the result expression,

$$\begin{aligned}
y =& \frac{1}{6}y^2_{i-1} + \frac{5}{3}y_{i-1}y_i + y_{i-1}y_{i+1} + \frac{4}{3}y^2_i + \frac{5}{3}y_{i-1}y_{i+1} + \frac{1}{6}y^2_{i+1} && \text{(E14)}\\
\varphi(y) =& \mathcal{T}^{(e)}_{\mathcal{P}_n}\mathcal{T}^{(o)}_{\mathcal{P}_n}(x^2_{2i-1} + 4x_{2i-1}x_{2i} + x^2_{2i}) && \text{(E15)}
\end{aligned}$$

Thus, we get that

$$\mathcal{B}_{\mathcal{P}_n}(x^2_{2i-1} + 4x_{2i-1}x_{2i} + x^2_{2i}) \subset \varphi(\mathcal{P}_N), \tag{E16}$$

which complete the proof of statement E8.

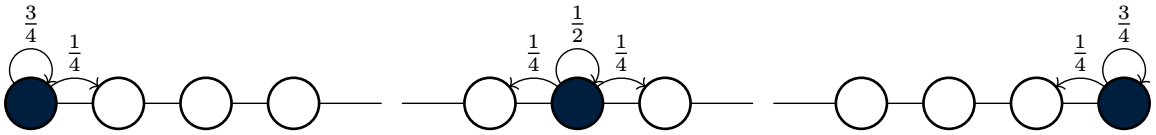

FIG. 6: Illustration of lazy symmetry random walk.

We aim to show that $\varphi(\mathcal{P}_N)$ is a faithful sub-representation. Suppose, for the sake of contradiction, that $\varphi(\mathcal{P}_N)$ is not faithful. Then, there exists a non-zero element $y \in \mathcal{P}_N$ such that:

$$\varphi(y) \neq 0 \quad \text{and} \quad \mathcal{B}^t_{\mathcal{P}_n}(\varphi(y)) = 0 \quad \text{for some integer } t \geq 1.$$

Consider applying the operator $\mathcal{B}^{t'}_{\mathcal{P}_n}$ iteratively to both sides of the equation:

$$\mathcal{B}^{t'}_{\mathcal{P}_n}\left[\mathcal{B}^{t}_{\mathcal{P}_n}(\varphi(y))\right] = \mathcal{B}^{t+t'}_{\mathcal{P}_n}(\varphi(y)) = \mathcal{B}^{t'}_{\mathcal{P}_n}(0) = 0.$$

Taking the limit as $t' \to \infty$, we obtain:

$$\lim_{t'\to\infty} \mathcal{B}^{t+t'}_{\mathcal{P}_n}(\varphi(y)) = 0.$$

However, the infinite application of $\mathcal{B}_{\mathcal{P}_n}$ to $\varphi(y)$ yields a non-zero polynomial. This is a contradiction because the same expression cannot simultaneously be zero and non-zero. Therefore, our initial assumption that $\varphi(\mathcal{P}_N)$ is not faithful must be false. Hence, $\varphi(\mathcal{P}_N)$ is indeed a faithful sub-representation.

□

2. Mapping the spread of polynomials to random walk

The action of layers is the lazy-symmetry random walk on a 2D square lattice in most sites. To illustrate this point, we will begin with a specific example. Considering $1 < i < N-1$ and $i+1 < j \leq N$, the action of $\mathcal{B}_{\mathcal{P}_N}$ is

$$\mathcal{B}_{\mathcal{P}_N}(y_i y_j) = \left(\frac{1}{4}y_{i-1} + \frac{1}{2}y_i + \frac{1}{4}y_{i-1}\right)\left(\frac{1}{4}y_{j-1} + \frac{1}{2}y_j + \frac{1}{4}y_{j-1}\right). \tag{E17}$$

In this case, the action of $\mathcal{B}_{\mathcal{P}_N}$ can be viewed as first independently evolving y_i and y_j in a one-dimensional lattice, and then combining them,

$$\begin{aligned} y_i &\to \frac{1}{4}y_{i-1} + \frac{1}{2}y_i + \frac{1}{4}y_{i-1} \\ y_j &\to \frac{1}{4}y_{j-1} + \frac{1}{2}y_j + \frac{1}{4}y_{j-1}. \end{aligned} \tag{E18}$$

We observe that this pattern appears in most sites $y_i y_j$. Therefore, we can analyze the evolving behavior separately in one-dimensional polynomial space (one-dimensional lattice). Afterward, we can examine the differences between the true evolved polynomial and the combined polynomial. This approach is the skeleton of estimating the order of tensor contraction. Now, we will make the above concepts more specific and more concrete.

We introduce the lazy-symmetry random walk in polynomial space, or the one-dimensional lattice, to describe the separate evolution behavior. A lazy-symmetry random walk is a type of Markov process shown in Fig. **??**. In this process, consider a point located at a site y_i. In the next time interval, this point has a probability of 0.25 moving to one of its neighboring sites y_{i-1} or y_{i+1}, and it has a probability of 0.5 staying in place. If the origin site is on the ends of the lattice, it has a probability of 0.75 staying in place and has a probability of 0.25 moving around. The probability transition relation could be expressed by

$$L\left(y_i\right) = \begin{cases} \frac{3}{4}y_1 + \frac{1}{4}y_2, & i = 1 \\ \frac{1}{4}y_{i-1} + \frac{1}{2}y_i + \frac{1}{4}y_{i+1}, & 1 < i < N \\ \frac{3}{4}y_N + \frac{1}{4}y_{N-1}, & i = N. \end{cases} \tag{E19}$$

y_iy_j	$\mathcal{B}_{\mathcal{P}_N}(y_iy_j)$
$i=j=1$	$L(y_i)L(y_j)-\frac{5}{144}y_1y_1-\frac{5}{144}y_2y_2+\frac{5}{72}y_1y_2$
$1<i<N, j=i$	$L(y_i)L(y_j)-\frac{5}{144}y_{i-1}y_{i-1}+\frac{1}{36}y_{i-1}y_i+\frac{1}{24}y_{i-1}y_{i+1}-\frac{1}{36}y_iy_i+\frac{1}{36}y_iy_{i+1}-\frac{5}{144}y_{i+1}y_{i+1}$
$1\leq i<N, j=i+1$	$L(y_i)L(y_j)-\frac{1}{48}y_iy_i-\frac{1}{48}y_{i+1}y_{i+1}+\frac{1}{24}y_iy_{i+1}$
$i=j=N$	$L(y_i)L(y_j)-\frac{5}{144}y_Ny_N-\frac{5}{144}y_{N-1}y_{N-1}+\frac{5}{72}y_{N-1}y_N$
other case	$L(y_i)L(y_j)$

TABLE II: The transition result of $\mathcal{B}_{\mathcal{P}_N}$ with input y_iy_j in different condition. Notice that $y_iy_j = y_jy_i$, the indices of the two factors i and j in term y_iy_j can always be arranged in ascending order $i\leq j$.

We could see that the separate evolution in Eq. (E18) fits the form of lazy-symmetry random walk. The transition step $\mathcal{L}_{\Gamma_2}$ in the representation space Γ_2' could be given by

$$\mathcal{L}_{\Gamma_2}|\gamma_S,\gamma_S\rangle\rangle=(L\times L)\circ\varphi'\circ\phi(|\gamma_S,\gamma_S\rangle\rangle), \tag{E20}$$

where $(L\times L)(y_iy_j)=L(y_i)L(y_j)$.

In Eq. (E17), we showed the result of how y_iy_j transfers in one specific situation. Now, we will show all possible results in any situation in Table II. The table lists all the possible transition results no matter what inputs it receives. It was created in a similar way to the previous example in Eq. (E13).

In Table II, we can see that in most cases

$$\mathcal{B}_{\mathcal{P}_N}(y_iy_j)=L(y_i)L(y_j) \tag{E21}$$

except for the cases when $|i-j|\leq 1$. Moreover, the coefficients of remainder terms $\mathcal{B}_{\mathcal{P}_N}(y_iy_j)-L(y_i)L(y_j)$ are small. Refs. [21] gives the analytical solution of lazy-symmetry random walk,

$$L^t(y_i)=\sum_\mu \mathcal{L}_i(\mu,t)y_\mu, \tag{E22}$$

where $L^t(y_i)$ represents the outcome of random walking $\mathcal{T}$ steps from y_i according to the propagation rule L in Eq. (E19), and the $\mathcal{L}_i(\mu,t)$ represents the probability of stopping at y_μ after $\mathcal{T}$-steps random walking,

$$\mathcal{L}_i(\mu,t)=\frac{1}{N}+\frac{2}{N}\sum_{k=1}^{N-1}\cos\left(\left(\mu-\frac{1}{2}\right)\frac{\pi k}{N}\right)\cos\left(\left(i-\frac{1}{2}\right)\frac{\pi k}{N}\right)\cos^{2t}\left(\frac{\pi k}{2N}\right). \tag{E23}$$

Thus, for the evolution that could be separated by $\mathcal{B}_{\mathcal{P}_N}(y_iy_j)=L(y_i)L(y_j)$, we could get the analytical solution results

$$\begin{aligned}\mathcal{C}^{\mathcal{P}_N}(t)(y_iy_j)=&(\mathcal{B}_{\mathcal{P}_N})^t(y_iy_j) &\text{(E24)}\\ =&L^t(y_i)L^t(y_j)+R(y_iy_j) &\text{(E25)}\\ =&\sum_{\mu,\nu}\left(\mathscr{L}_{ij}(\mu,\nu,t)y_\mu y_\nu+\mathscr{R}_{ij}(\mu,\nu,t)y_\mu y_\nu\right), &\text{(E26)}\end{aligned}$$

where

$$\mathscr{L}_{ij}(\mu,\nu,t):=\mathcal{L}_i(\mu,t)\mathcal{L}_j(\nu,t). \tag{E27}$$

The R stands for the reminder terms caused by the near-diagonal terms y_iy_j, $|i-j|\leq 1$ in Table II.

The calculation of α can be divided into two parts. The first part comes from the lazy-symmetry random walk, and the second part comes from the remainder terms. Recall that $\alpha_{S,d}$ is calculated by the tensor contraction of $\mathcal{C}$, $|P_S\rangle\rangle$, and $|\mathbf{0},\mathbf{0}\rangle\rangle$. We have mapped both $\mathcal{C}$ and $|P_S\rangle\rangle$ into polynomial space. Similarly, $|\mathbf{0},\mathbf{0}\rangle\rangle$ is also mapped into polynomial space.

Equation (D4) transforms $|\mathbf{0},\mathbf{0}\rangle\rangle$ into the Pauli basis. Notice that $\langle\langle Z_i|$ is a linear function that converts a super vector into a number. Specifically, it maps $|Z_i\rangle\rangle$ to 1 and maps other Pauli basis vectors to 0. As mentioned earlier, $|Z_i\rangle\rangle$ is mapped to x_i^2 in $\mathcal{P}_n$. The derivative operators' space is the polynomial space's dual space. Therefore, we use the space of derivative operators to represent the dual space of $\mathcal{P}_n$

$$\langle\langle\psi_{ij}| \to \frac{\partial^2}{\partial x_i \partial x_j}, \quad \langle\langle\psi_{ii}| \to \frac{1}{2}\frac{\partial^2}{\partial x_i^2}. \tag{E28}$$

With similar methods and some algebra, we map the $\langle\langle\mathbf{0},\mathbf{0}|$ to $\mathcal{P}_N$ when $|S|=2$

$$\langle\langle\mathbf{0},\mathbf{0}| \to \frac{1}{2^{2n}}\frac{1}{6}\sum_{i,j}\frac{\partial^2}{\partial y_i^2}. \tag{E29}$$

Thus, the $\alpha_{S,2t+1}$ could be expressed as

$$\alpha_{\{\gamma_i\gamma_j\},2t+1} = \frac{1}{6}\sum_{\mu}\frac{\partial^2}{\partial y_\mu^2}\mathcal{C}^{\mathcal{P}_N}(t)(y_i y_j). \tag{E30}$$

Then, we could calculate $\alpha_{S,d}$ by a random walk in $\mathcal{P}_N$ via combining Eq. (E26) and Eq. (E30)

$$\begin{aligned}\alpha_{\{\gamma_i\gamma_j\},2t+1} =& \frac{1}{3}\sum_{\mu}\mathscr{L}_{ij}(\mu,\mu,t) + \frac{1}{3}\sum_{\mu}\mathscr{R}_{ij}(\mu,\mu,t) &\text{(E31)}\\ =:& \alpha^L_{\{\gamma_i\gamma_j\},2t+1} + \alpha^R_{\{\gamma_i\gamma_j\},2t+1}. &\text{(E32)}\end{aligned}$$

The term $\mathscr{L}_{ij}(\mu,\mu,t)$ is a transition probability.

Appendix F: Estimate the order of $\alpha^L_{\{\gamma_i\gamma_j\},2t+1}$

We have separated the calculation of $\alpha_{\{\gamma_i\gamma_j\},2t+1}$ into two parts in Sec. E 2. In this section, we aim to estimate the order of the first part, $\alpha^L_{\{\gamma_i\gamma_j\},2t+1}$.

Lemma 4. *The $\alpha^L_{\{\gamma_i\gamma_j\},2t+1}$ could be estimated by the following formula*

$$\alpha^L_{\{\gamma_i\gamma_j\},2t+1} = \frac{1}{3\sqrt{2\pi t}}\sum_{k=-\infty}^{\infty}\left(e^{-\frac{(2Nk+a)^2}{2t}} + e^{-\frac{(2Nk+b)^2}{2t}}\right) + \mathcal{O}\left(e^{-\frac{\pi^2}{2}t}\right) \tag{F1}$$

where a is defined as $|i-j|$ and b is defined as $i+j-1$.

Proof. Recall that $N = n/2$. By Lemma 5, we could simplify the expression of $\alpha^L_{\{\gamma_i\gamma_j\},2t+1}$ into Eq. (F8). Then, we absorb the $k=0$ into the summation

$$\begin{aligned}3\alpha^L_{\{\gamma_i\gamma_j\},2t+1} &= \frac{1}{N} + \frac{1}{N}\sum_{k=1}^{N-1}\left[\cos\left((i-j)\frac{k\pi}{N}\right) + \cos\left((i+j-1)\frac{k\pi}{N}\right)\right]\cos^{4t}\left(\frac{\pi k}{2N}\right)\\ &= -\frac{1}{N} + \frac{1}{N}\sum_{k=0}^{N-1}\left[\cos\left((i-j)\frac{k\pi}{N}\right) + \cos\left((i+j-1)\frac{k\pi}{N}\right)\right]\cos^{4t}\left(\frac{\pi k}{2N}\right).\end{aligned} \tag{F2}$$

In this way, the summation over k will go through a complete cycle period. This will allow us to utilize some useful properties regarding trigonometric summations.

We aim to use the Poison summation formula to estimate the order of $\alpha^L_{\{\gamma_i\gamma_j\},2t+1}$. Thus, it is more convenient to express the formula by exponentials rather than trigonometric functions. Notice that the e^{-2tx^2} is a good estimation of $\cos^{4t}(x)$

$$\begin{aligned}& e^{-2tx^2} - \cos^{4t}(x)\\ =& e^{-2tx^2} - e^{-2tx^2+O\left(tx^4\right)}\\ =& e^{-2tx^2}\left(1 - e^{O\left(tx^4\right)}\right)\\ \sim& \mathcal{O}\left(tx^4 e^{-2tx^2}\right).\end{aligned} \tag{F3}$$

Substitute $\cos^{4t}\left(\frac{\pi k}{2N}\right)$ with $e^{-\frac{k^2\pi^2 t}{2N^2}}$ in Eq. (F16), we have

$$3\alpha^L_{\{\gamma_i\gamma_j\},2t+1} = -\frac{1}{N} + \frac{1}{N}\sum_{k=0}^{N-1} e^{-\frac{k^2\pi^2 t}{2N^2}}\left[\cos\left((i-j)\frac{k\pi}{N}\right) + \cos\left((i+j-1)\frac{k\pi}{N}\right)\right] + \mathcal{O}\left(e^{-\frac{\pi^2}{2}t}\right) \tag{F4}$$

$$= -\frac{1}{N} + \frac{1}{N}\sum_{k=0}^{\infty} e^{-\frac{k^2\pi^2 t}{2N^2}}\left[\cos\left((i-j)\frac{k\pi}{N}\right) + \cos\left((i+j-1)\frac{k\pi}{N}\right)\right] + \mathcal{O}\left(e^{-\frac{\pi^2}{2}t}\right). \tag{F5}$$

In the second line, we expand the summation to infinity, and it will not introduce much of errors because

$$\begin{aligned}
\sum_{k=N}^{\infty} e^{-\frac{k^2\pi^2 t}{2N^2}} =& e^{-\frac{\pi^2}{2}t}\sum_{k=0}^{\infty} e^{-\frac{k^2\pi^2 t}{2N^2}} \\
\leq& e^{-\frac{\pi^2}{2}t}\sum_{k=0}^{\infty} e^{-\frac{k\pi^2 t}{2N^2}} \\
=& e^{-\frac{\pi^2}{2}t}\frac{e^{\frac{\pi^2 t}{2N^2}}}{e^{\frac{\pi^2 t}{2N^2}}-1} \\
=& \mathcal{O}\left(e^{-\frac{\pi^2}{2}t}\right)
\end{aligned}$$

According to the Poison summation formula,

$$\sum_{k=-\infty}^{\infty} e^{-\frac{k^2\pi^2 t}{2N^2}}\cos\left((i-j)\frac{k\pi}{N}\right) = N\sqrt{\frac{2}{\pi t}}\sum_{k=-\infty}^{\infty} e^{-\frac{(2Nk+i-j)^2}{2t}} \tag{F6}$$

Substitute the Eq. (F6) into Eq. (F5), we have

$$\alpha^L_{\{\gamma_i\gamma_j\},2t+1} = \frac{1}{3\sqrt{2\pi t}}\sum_{k=-\infty}^{\infty}\left(e^{-\frac{(2Nk+i-j)^2}{2t}} + e^{-\frac{(2Nk+i+j-1)^2}{2t}}\right) + \mathcal{O}\left(e^{-\frac{\pi^2}{2}t}\right). \tag{F7}$$

□

We can therefore conclude that the value of $\alpha^L_{\{\gamma_i\gamma_j\},2t+1}$ will be on the order of $\frac{1}{\text{poly}(n)}$ if $\mathcal{T}$ is of the same order magnitude as a^2.

Lemma 5. *The expression of $\alpha^L_{\{\gamma_i\gamma_j\},2t+1}$ could be simplified to the following form*

$$3\alpha^L_{\{\gamma_i\gamma_j\},2t+1} = \frac{1}{N} + \frac{1}{N}\sum_{k}\left[\cos\left((i-j)\frac{k\pi}{N}\right) + \cos\left((i+j-1)\frac{k\pi}{N}\right)\right]\cos^{4t}\left(\frac{\pi k}{2N}\right). \tag{F8}$$

Proof. The lemma will be proved by directly calculation.

$$\begin{aligned}
3\alpha^L_{\{\gamma_i\gamma_j\},2t+1} =& \sum_{\mu}\left[\frac{1}{N} + \frac{2}{N}\sum_{k=1}^{N-1}\cos\left(\left(i-\frac{1}{2}\right)\frac{\pi k}{N}\right)\cos\left(\left(\mu-\frac{1}{2}\right)\frac{\pi k}{N}\right)\cos^{2t}\left(\frac{\pi k}{2N}\right)\right] \\
&\times\left[\frac{1}{N} + \frac{2}{N}\sum_{l=1}^{N-1}\cos\left(\left(j-\frac{1}{2}\right)\frac{\pi l}{N}\right)\cos\left(\left(\mu-\frac{1}{2}\right)\frac{\pi l}{N}\right)\cos^{2t}\left(\frac{\pi l}{2N}\right)\right] \\
=& 1/N + \frac{2}{N^2}\sum_{k}\left[\sum_{\mu}\cos\left(\left(\mu-\frac{1}{2}\right)\frac{\pi k}{N}\right)\right]\cos\left(\left(i-\frac{1}{2}\right)\frac{\pi k}{N}\right)\cos^{2t}\left(\frac{\pi k}{2N}\right) &\text{(F9)} \\
&+ \frac{2}{N^2}\sum_{l}\left[\sum_{\mu}\cos\left(\left(\mu-\frac{1}{2}\right)\frac{\pi l}{N}\right)\right]\cos\left(\left(i-\frac{1}{2}\right)\frac{\pi l}{N}\right)\cos^{2t}\left(\frac{\pi l}{2N}\right) &\text{(F10)} \\
&+ \frac{4}{N^2}\sum_{k,l=1}^{N-1}\sum_{\mu=1}^{N}\cos\left(\left(i-\frac{1}{2}\right)\frac{\pi k}{N}\right)\cos\left(\left(\mu-\frac{1}{2}\right)\frac{\pi k}{N}\right)\cos^{2t}\left(\frac{\pi k}{2N}\right) \\
&\times\cos\left(\left(j-\frac{1}{2}\right)\frac{\pi l}{N}\right)\cos\left(\left(\mu-\frac{1}{2}\right)\frac{\pi l}{N}\right)\cos^{2t}\left(\frac{\pi l}{2N}\right) &\text{(F11)}
\end{aligned}$$

Notice that the summation of cosin function is zero

$$\begin{aligned}\sum_{\mu=1}^{N}\cos\left(\left(\mu-\frac{1}{2}\right)\frac{\pi k}{N}\right)&=-\frac{1}{2}\cos\left(\frac{1}{2}\pi(2k+1)\right)\csc\left(\frac{\pi k}{2N}\right)\\&=\sin(k\pi)\csc\left(\frac{\pi k}{2N}\right)\\&=0.\end{aligned}\tag{F12}$$

Substitute this identity into Eq. (F11), we could eliminate the terms in line (F9) and (F10).

Also, notice that

$$\begin{aligned}&\sum_{\mu=1}^{N}\cos\left(\frac{\pi\left(\mu-\frac{1}{2}\right)i}{N}\right)\cos\left(\frac{\pi\left(\mu-\frac{1}{2}\right)j}{N}\right)\\=&\frac{1}{2}\sum_{\mu=1}^{N}\cos\left(\frac{\pi\left(\mu-\frac{1}{2}\right)i}{N}-\frac{\pi\left(\mu-\frac{1}{2}\right)j}{N}\right)+\cos\left(\frac{\pi\left(\mu-\frac{1}{2}\right)i}{N}+\frac{\pi\left(\mu-\frac{1}{2}\right)j}{N}\right)\\=&\frac{1}{2}\sum_{\mu=1}^{N}\cos\left(\frac{\pi(2\mu-1)(i-j)}{2N}\right)+\cos\left(\frac{\pi(2\mu-1)(i+j)}{2N}\right)\\=&\frac{1}{4}\left(\sin(\pi(i+j))\csc\left(\frac{\pi(i+j)}{2N}\right)-\sin(\pi(j-i))\csc\left(\frac{\pi(i-j)}{2N}\right)\right).\end{aligned}\tag{F13}$$

This result gets value 0 when $\frac{\pi(i+j)}{2N}\neq a\pi$ or $\frac{\pi(i-j)}{2N}\neq b\pi$ for some integer a and b, because $\sin(\pi m)=0$. The term $\sin(\pi m)\csc\left(\frac{\pi m}{2N}\right)$ gets non-zero only when $\csc\left(\frac{\pi m}{2N}\right)$ gets infinity. Then, we could write down the conditions that i and j satisfy

$$\begin{cases}i+j=2aN \text{ or } |i-j|=2bN\\ a,b\in\mathbb{Z}\\ 1<i,j<N-1.\end{cases}\tag{F14}$$

The equation shows that the result is $j=k$. We can use L'Hôpital's rule to calculate the term

$$\lim_{x\to 0}\sin(\pi x)\csc\left(\frac{\pi x}{2N}\right)=2N\tag{F15}$$

when i and j satisfy the condition $i=j$. Plugin Eq. (F15) and Eq. (F13) into Eq. (F11), we have

$$3\alpha^{L}_{\{\gamma_i\gamma_j\},2t+1}=\frac{1}{N}+\frac{2}{N}\sum_{k}\cos\left(\left(i-\frac{1}{2}\right)\frac{\pi k}{N}\right)\cos\left(\left(j-\frac{1}{2}\right)\frac{\pi k}{N}\right)\cos^{4t}\left(\frac{\pi k}{2N}\right).\tag{F16}$$

Finally, we use trigonometric identities to expand this equation, thereby completing this proof

$$3\alpha^{L}_{\{\gamma_i\gamma_j\},2t+1}=\frac{1}{N}+\frac{1}{N}\sum_{k}\left[\cos\left((i-j)\frac{k\pi}{N}\right)+\cos\left((i+j-1)\frac{k\pi}{N}\right)\right]\cos^{4t}\left(\frac{\pi k}{2N}\right).\tag{F17}$$

□

Appendix G: The relation between $\alpha^{L}_{\{\gamma_i\gamma_j\},2t+1}$ and $\alpha^{R}_{\{\gamma_i\gamma_j\},2t+1}$

Recall that we have divided the calculation of $\alpha_{\{\gamma_i\gamma_j\},2t+1}$ into two parts. One is the $\alpha^{L}_{\{\gamma_i\gamma_j\},2t+1}$ and the other is $\alpha^{R}_{\{\gamma_i\gamma_j\},2t+1}$. Theorem 4 gives the order of $\alpha^{L}_{\{\gamma_i\gamma_j\},2t+1}$. In this section, we aim to bound the $\alpha^{R}_{\{\gamma_i\gamma_j\},2t+1}$ by $\alpha^{L}_{\{\gamma_i\gamma_j\},2t+1}$, so that the order of $\alpha_{\{\gamma_i\gamma_j\},2t+1}$ could be given by the $\alpha^{L}_{\{\gamma_i\gamma_j\},2t+1}$.

We begin with the polynomial in Eq. (E26)

$$\mathcal{C}^{\mathcal{P}_N}(t)(y_iy_j)=\sum_{\mu,\nu}\left(\mathscr{L}_{ij}(\mu,\nu,t)y_\mu y_\nu+\mathscr{R}_{ij}(\mu,\nu,t)y_\mu y_\nu\right).\tag{G1}$$

Then, we let the polynomial transform one time-interval step, and we get

$$\mathcal{C}^{\mathcal{P}_N}(t+1)(y_iy_j) \tag{G2}$$
$$=\mathcal{B}_{\mathcal{P}_N}\left(\mathcal{C}^{\mathcal{P}_N}(t)(y_iy_j)\right) \tag{G3}$$
$$=\sum_{\mu,\nu}\left(\mathscr{L}_{ij}(\mu,\nu,t)(L(y_\mu)L(y_\nu)+R(y_\mu,y_\nu))+\mathscr{R}_{ij}(\mu,\nu,t)(L(y_\mu)L(y_\nu)+R(y_\mu,y_\nu))\right) \tag{G4}$$
$$=\sum_{\mu,\nu}\left(\mathscr{L}_{ij}(\mu,\nu,t)(L(y_\mu)L(y_\nu)+R(y_\mu,y_\nu))+\mathscr{R}_{ij}(\mu,\nu,t)(L(y_\mu)L(y_\nu)+R(y_\mu,y_\nu))\right) \tag{G5}$$
$$=\sum_{\mu,\nu}\mathscr{L}_{ij}(\mu,\nu,t+1)y_\mu y_\nu+\sum_{\mu,\nu}\mathscr{L}_{ij}(\mu,\nu,t)R(y_\mu,y_\nu)$$
$$+\sum_{\mu,\nu}\mathscr{R}_{ij}(\mu,\nu,t)(L(y_\mu)L(y_\nu)+R(y_\mu,y_\nu)). \tag{G6}$$

Deduce from Eq. (G1), we have

$$\mathcal{C}^{\mathcal{P}_N}(t+1)(y_iy_j)=\sum_{\mu,\nu}\left(\mathscr{L}_{ij}(\mu,\nu,t+1)y_\mu y_\nu+\mathscr{R}_{ij}(\mu,\nu,t+1)y_\mu y_\nu\right). \tag{G7}$$

Compare Eq. (G6) and Eq. (G7), we have

$$\sum_{\mu,\nu}\mathscr{R}_{ij}(\mu,\nu,t+1)y_\mu y_\nu=\sum_{\mu,\nu}\mathscr{L}_{ij}(\mu,\nu,t)R(y_\mu,y_\nu)+\sum_{\mu,\nu}\mathscr{R}_{ij}(\mu,\nu,t)(L(y_\mu)L(y_\nu)+R(y_\mu,y_\nu)) \tag{G8}$$
$$(1+\delta_{l,k})\mathscr{R}_{ij}(l,k,t+1)=\sum_{\mu,\nu}\mathscr{R}_{ij}(\mu,\nu,t)\frac{\partial^2L(y_\mu)L(y_\nu)}{\partial y_l\partial y_k}+\sum_{\mu,\nu}\left(\mathscr{L}_{ij}(\mu,\nu,t)+\mathscr{R}_{ij}(\mu,\nu,t)\right)\frac{\partial^2R(y_\mu,y_\nu)}{\partial y_l\partial y_k}. \tag{G9}$$

Eq. (G9) describes the strict relationship between $\mathscr{R}_{ij}$ and $\mathscr{L}_{ij}$ in a recursive form, thereby giving the relationship between $\alpha^L_{\{\gamma_i\gamma_j\},2t+1}$ and $\alpha^R_{\{\gamma_i\gamma_j\},2t+1}$. However, deriving the general term formula from this recursive formula is difficult. Therefore, we hope to use some inequalities to simplify this recursive relationship and thus bound $\alpha^R_{\{\gamma_i\gamma_j\},2t+1}$ by $\alpha^L_{\{\gamma_i\gamma_j\},2t+1}$.

We will first define some auxiliary variables,

$$\zeta_k(t):=\frac{1}{2}\sum_{\mu=1}^{N-k}\left(\mathcal{L}_i(\mu,t)\mathcal{L}_j(\mu+k,t)+\mathcal{L}_i(\mu+k,t)\mathcal{L}_j(\mu,t)\right)$$
$$\beta_k(t):=\frac{1}{2}\sum_{\mu=1}^{N-k}\left(\mathscr{R}_{i,j}(\mu,\mu+k,t)+\mathscr{R}_{i,j}(\mu+k,\mu,t)\right)$$
$$a(t):=\begin{pmatrix}\zeta_0(t)\\ \zeta_1(t)\end{pmatrix},\quad b(t):=\begin{pmatrix}\beta_0(t)\\ \beta_1(t)\end{pmatrix}.$$

Notice that $3\alpha^L_{\{\gamma_i\gamma_j\},2t+1}=\zeta_0(t)$, $3\alpha^R_{\{\gamma_i\gamma_j\},2t+1}=\beta_0(t)$. Because $\mathscr{L}_{i,j}(\mu,\nu,t)+\mathscr{R}_{i,j}(\mu,\nu,t)$ represents the probability of being in site y_iy_j during a random walk, it satisfies the property that the summation across all sites is 1. Meanwhile, the summation of all $\mathscr{L}_{i,j}(\mu,\nu,t)$ is 1. The two things deduce that

$$\sum_{\mu,\nu}\mathscr{R}_{i,j}(\mu,\nu,t)=0. \tag{G10}$$

Especially, in numerical simulation, we observe that all $\mathscr{R}_{i,j}(\mu,\nu,t)$ are greater than 0 except for $\mu=\nu$. The numerical results are shown in Fig. 7. Under this assumption, we have the following lemma:

Lemma 6. *Assume that* $\forall\mu\neq\nu$, $\mathscr{R}_{i,j}(\mu,\nu,t)<0$, *and* $\forall\mu\neq\nu$, $\mathscr{R}_{i,j}(\mu,\mu,t)>0$. $-\beta_0(t)\leq\frac{25}{72}\max_{k\geq0}\{\zeta_0(t-k)\}$.

Theorem 6 establishes the mathematical relationship between the two components $\alpha^L_{\{\gamma_i\gamma_j\},2t+1}$ and $\alpha^R_{\{\gamma_i\gamma_j\},2t+1}$. By combining this theoretical relationship with the equality described in Eq. (E32), we can deduce the order of magnitude of the $\alpha_{\{\gamma_i\gamma_j\},2t+1}$. Combining these pieces allows us to systematically determine the scale or size of $\alpha_{\{\gamma_i\gamma_j\},2t+1}$ based on the other defined quantities.

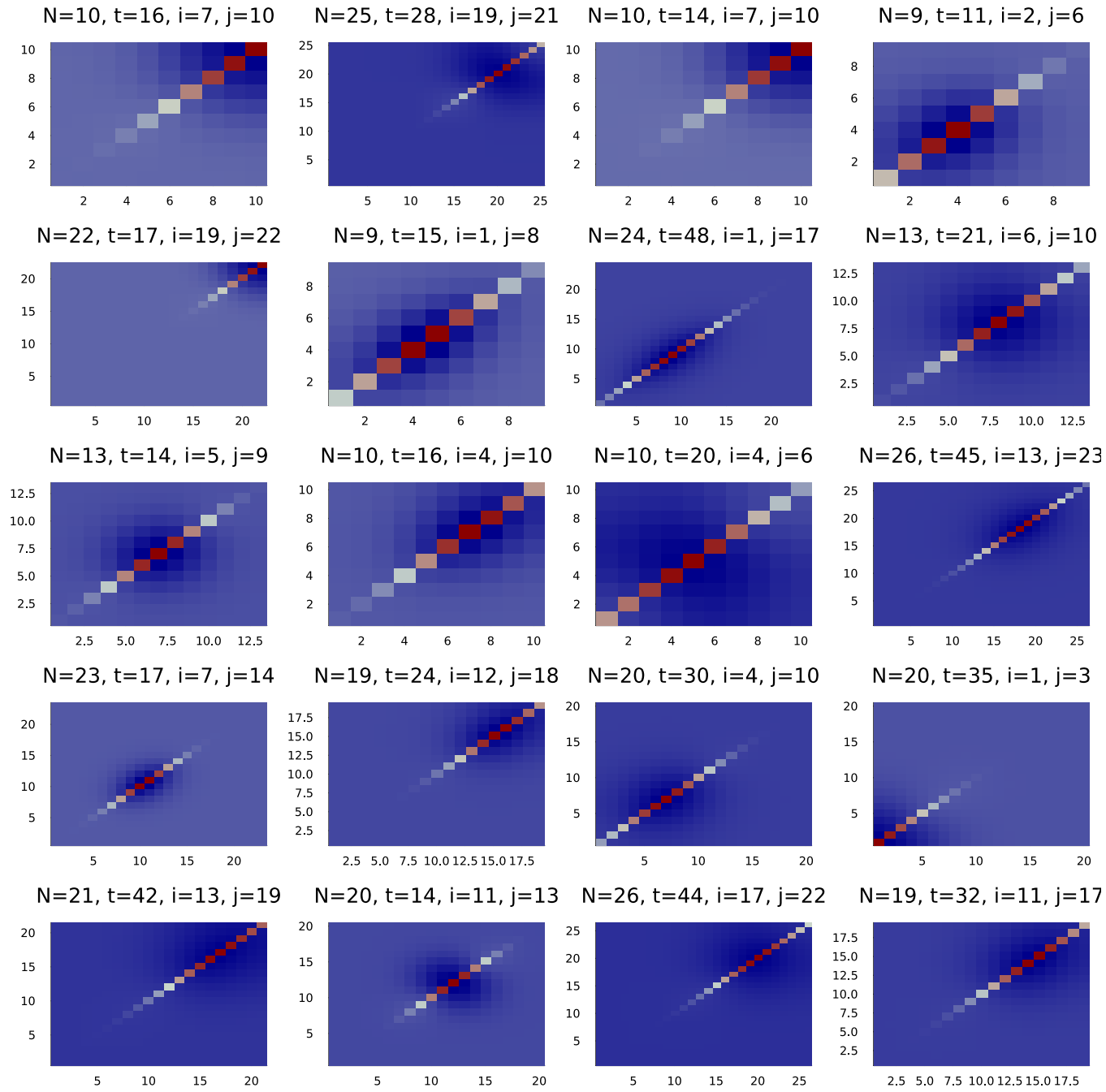

FIG. 7: The value of $\mathscr{R}_{i,j}(\mu,\nu,t)$. We randomly choose N,t,i,j, and calculate the value of $\mathscr{R}_{i,j}(\mu,\mu,t)$ numerically. The pixel is colored red if $\mathscr{R}_{i,j}(\mu,\nu,t)$ greater than 0, else the pixel is colored blue. The x-axis represents the μ and the y-axis represents the ν. The numerical results show that $\mathscr{R}_{i,j}(\mu,\mu,t) < 0$ when $\mu \neq \nu$.

proof of Lemma 6. From the recursive relationship in Eq. (G9) and Table II, we could write down the recursive

relationship of β_k

$$\begin{aligned}\beta_0(t+1) \geq & \frac{6}{16}\beta_0(t) + \frac{8}{16}\beta_1(t) + \frac{2}{16}\beta_2(t) - \frac{14}{144}\left(\beta_0(t)+\zeta_0(t)\right) - \frac{1}{24}\left(\beta_1(t)+\zeta_1(t)\right) \\ & + \frac{4}{16}(\mathscr{R}_{ij}(0,0,t-1) + \mathscr{R}_{ij}(N,N,t-1)) - \frac{1}{16}(\mathscr{R}_{ij}(0,1,t-1) + \mathscr{R}_{ij}(1,0,t-1)) \\ & - \frac{1}{16}(\mathscr{R}_{ij}(N-1,N,t-1) + \mathscr{R}_{ij}(N,N-1,t-1)) \\ \geq & \frac{5}{18}\beta_0(t) + \frac{11}{24}\beta_1(t) - \frac{7}{72}\zeta_0(t) - \frac{1}{12}\zeta_1(t) \qquad \text{(G11)} \\ \geq & \frac{5}{18}\beta_0(t) + \frac{5}{24}\beta_1(t) - \frac{7}{72}\zeta_0(t) - \frac{1}{12}\zeta_1(t) \qquad \text{(G12)}\end{aligned}$$

Here, we use the property that $\beta_0(t)+\zeta_0(t)$ is the summation of properties so that it is greater than 0 to inequality deflate the terms at the edges, like y_0y_0 or y_0y_1. Recall that we hold the assumption that $\mathscr{R}_{i,j}(\mu,\mu,t) < 0$, and $\forall \mu \neq \nu$, $\mathscr{R}_{i,j}(\mu,\mu,t) > 0$, so the edges terms of $\mathscr{R}_{ij}$ could be deflated out as well. Similarly, we have

$$\beta_1(t+1) \geq \frac{5}{9}\beta_0(t) + \frac{5}{12}\beta_1(t) + \frac{1}{18}\zeta_0(t) + \frac{1}{24}\zeta_1(t). \qquad \text{(G13)}$$

Let β_0' and β_1' obtains the above recursive relation

$$\begin{cases}\beta_0'(t+1) = & \frac{5}{18}\beta_0(t) + \frac{5}{24}\beta_1(t) - \frac{7}{72}\zeta_0(t) - \frac{1}{12}\zeta_1(t) \\ \beta_1'(t+1) = & \frac{5}{9}\beta_0(t) + \frac{5}{12}\beta_1(t) + \frac{1}{18}\zeta_0(t) + \frac{1}{24}\zeta_1(t)\end{cases} \qquad \text{(G14)}$$

with the same first term $\beta_0'(0) = \beta_0(0)$ and $\beta_1'(0) = \beta_1(0)$. The β and β' satisfy the relationship

$$\beta_0'(t) \geq \beta_0(t), \quad \beta_1'(t) \geq \beta_1(t). \qquad \text{(G15)}$$

Similarly, we denote b' as $b'(t) := \binom{\beta_0'(t)}{\beta_1'(t)}$,

We rewrite the inequality groups (G14) to the matrix form

$$b'(t+1) = C_b b'(t) + C_a a(t), \quad \text{where} \qquad \text{(G16)}$$

$$C_b = \begin{pmatrix} \frac{5}{18} & \frac{5}{24} \\ \frac{5}{9} & \frac{5}{12} \end{pmatrix}, \quad C_a = \begin{pmatrix} -\frac{7}{72} & -\frac{1}{12} \\ \frac{1}{18} & \frac{1}{24} \end{pmatrix}, \qquad \text{(G17)}$$

and the matrices C_b and C_a govern these recursive dynamics. To solve this recursion explicitly, we diagonalize the C_b matrix. This allows us to express the recursion in closed form,

$$b'(t) = C_b^t b'(0) + \sum_{k=0}^{t-1} C_b^k C_a a(t-k-1). \qquad \text{(G18)}$$

The term C_b^t could be calculated by eigenvalue decomposition $C_b = Q\Lambda Q^{-1}$, where $\Lambda = \mathrm{diag}(\frac{25}{36}, 0)$. The eigenvector corresponding to $\frac{25}{36}$ is $(2, \frac{3}{2})^T$. This allows us to express C_b^k and $C_b^k C_a$ in terms of eigenvalues and eigenvectors

$$C_b^k = \left(\frac{5}{6}\right)^{2k} \begin{pmatrix} 2 & \frac{3}{2} \\ 0 & 0 \end{pmatrix} \qquad \text{(G19)}$$

$$C_b^k C_a = \frac{1}{5}\left(\frac{5}{6}\right)^{2k} \begin{pmatrix} -\frac{1}{9} & -\frac{5}{48} \\ 0 & 0 \end{pmatrix} \qquad \text{(G20)}$$

for any $k > 0$.

The variables we care about are ζ_0 and β_0 because they are directly related to the $\alpha^L_{\{\gamma_i\gamma_j\},2t+1}$ and $\alpha^R_{\{\gamma_i\gamma_j\},2t+1}$. Thus, we mainly consider the first item of $C_b^t b'(0)$ and $C_b^k C_a a(t-k-1)$, which could be expressed in the following form

$$C_b^k C_a a(t-k-1) = \lambda_k \zeta_0(t-k-1) + \eta_k \zeta_1(t-k-1). \qquad \text{(G21)}$$

The λ_k and the η_k are coefficients

$$\begin{array}{ll} \lambda_k = -\frac{1}{45}\left(\frac{5}{6}\right)^{2k}, & \eta_k = -\frac{1}{48}\left(\frac{5}{6}\right)^{2k}, \quad \forall k > 0, \\ \lambda_0 = -\frac{7}{72}, & \eta_0 = -\frac{1}{12}. \end{array} \tag{G22}$$

Building on the previous relationships, we can now derive an explicit formula for $\beta_0'(t)$. From the expression for the first element of $C_b^k C_a a(t-k-1)$, we obtain

$$\beta_0'(t) = \sum_{k=0}^{t} \left(\lambda_k \zeta_0(t-k-1) + \eta_k \zeta_1(t-k-1)\right) \tag{G23}$$

We also know from the recursive relation of $\mathcal{L}_i$ that the state variables satisfy

$$\zeta_0(t+1) \geq \frac{3}{8}\zeta_0(t) + \frac{1}{2}\zeta_1(t). \tag{G24}$$

Leveraging this inequality into Eq. G23 allows us to place an upper bound on $\beta_0'(t)$

$$-\beta_0'(t) \leq -\sum_{k=1}^{t}\left(\lambda_k - \frac{3}{4}\eta_k + 2\eta_{k+1}\right)\zeta_0(t-k-1) + \frac{19}{72}\zeta_0(t) - \frac{1}{16}\zeta_0(t-1) \tag{G25}$$

$$\leq \sum_{k=1}^{t}\left(\frac{5}{6}\right)^{2k}\frac{307}{8640}\zeta_0(t-k-1) + \frac{19}{72}\zeta_0(t) - \frac{1}{16}\zeta_0(t-1) \tag{G26}$$

$$\leq \frac{25}{72}\max_{k\geq 0}\{\zeta_0(t-k)\} \tag{G27}$$

□

Appendix H: Efficiency when the distance of set is short

Lemma 7. *The expectation value of* $\mathrm{tr}(\rho\gamma_S)$ *can be obtained by using* $\mathrm{polylog}(n)$*-layers matchgate circuit within the Fermionic classical shadows protocol, when the distance of* S *is* $\mathcal{O}(\log n)$ *and the cardinal number* $|S|$ *is a constant* $2c$*.*

Proof. Let the initial tensor be P_S, and apply $\mathcal{C}$ to the tensor P_S. Each $\mathcal{T}^{(e)}\mathcal{T}^{(o)}$ in $\mathcal{C}$ will transform the P_S to the superposition of a series of Pauli tensors

$$\mathcal{T}^{(e)}\mathcal{T}^{(o)}P_S = \sum_{|S'|=|S|}\xi_{S'}|P^{S'}\rangle\rangle, \tag{H1}$$

where $\xi_{S'}$ are real coefficients that satisfy $\sum\xi_{S'} = 1$. Now, we only preserve the branches S' which has smaller distance $d(S') < d(S)$ unless $d(S) = 1$. The condition $d(S) = 1$ means that

$$P_S = \prod_{i\in\Lambda} Z_i \tag{H2}$$

via Jordan-Wigner transformation. Only the Pauli basis in the form of $\prod_{i\in\Lambda} Z_i$ have non-zero inner product with $|\mathbf{0},\mathbf{0}\rangle\rangle$, which we explain it in Sec. E 2.

Table I tells us that the summation of the coefficients of remaining branches is greater than $\frac{1}{9^{|S|}}$. We apply $\mathcal{T}^{(e)}\mathcal{T}^{(o)}$ $d(S)/2$-times, and in each step, only remain the branches with smaller cardinal numbers. Afterward, the summation of coefficients of remained branches is greater than $\frac{1}{9^{|S|d(S)/2}}$. Notice that $|S|$ is a constant number and $d(S) = \mathcal{O}(\log(n))$, the summation number is

$$\sum_{S''}\xi_{S''} \geq \frac{1}{9^{\mathcal{O}(\log(n))}} = \frac{1}{\mathcal{O}(\mathrm{poly}(n))}, \tag{H3}$$

where S'' are the remained branches. □